Eur J Nucl Med Mol Imaging (2007) 34:448–452
DOI 10.1007/s00259-006-0256-6

ORIGINAL ARTICLE

Is MIBG a substrate of P-glycoprotein?

Yasushi Kiyono · Tomoko Yamashita · Hisako Doi · Yuji Kuge · Toshiya Katsura · Ken-Ichi Inui · Hideo Saji

Received: 5 February 2006 / Accepted: 30 July 2006 / Published online: 10 November 2006

Abstract
Purpose Radionuclide therapy with ^{131}I-labelled meta-iodobenzylguanidine ([^{131}I]MIBG) is effective in cases where it is difficult to carry out surgical resection or debulking of neuroendocrine tumours (NETs). However, it has recently been reported that P-glycoprotein (P-gp) is expressed in these NETs. Therefore, it is important to clarify whether MIBG is a substrate of P-gp or not. In this study, using a human cell line which overexpresses P-gp, LLC-GA5-COL150, we investigated this question.
Methods The transcellular transport and accumulation of [^{125}I]MIBG were measured using monolayer cultures grown in Transwell chambers. [^{125}I]MIBG was added to either the basolateral or the apical side, aliquots of the incubation medium on the other side were taken at specified times, and the radioactivity was measured. For accumulation experiments, the cells on the filters were solubilised and the radioactivity in aliquots was measured.
Results There were no significant differences in the transport of MIBG between LLC-PK$_1$ and LLC-GA5-COL150 monolayers in either direction until 60 min. With respect to the accumulation of MIBG, there were no significant differences between LLC-PK$_1$ and LLC-GA5-COL150 cells in either direction.
Conclusion MIBG is not a substrate of P-gp. Therefore, radionuclide therapy with MIBG would be useful in the treatment of NETs expressing P-gp.

Keywords [^{131}I]MIBG · P-glycoprotein · Transporter · Neuroendocrine tumour · Radionuclide therapy

Y. Kiyono
Radioisotopes Research Laboratory, Faculty of Medicine,
Kyoto University Hospital, Kyoto University,
Kyoto, Japan

T. Yamashita · H. Doi · Y. Kuge · H. Saji (✉)
Department of Patho-functional Bioanalysis,
Graduate School of Pharmaceutical Sciences, Kyoto University,
Sakyo-ku,
Kyoto 606-8501, Japan
e-mail: hsaji@pharm.kyoto-u.ac.jp

T. Katsura · K.-I. Inui
Department of Pharmacy, Faculty of Medicine,
Kyoto University Hospital, Kyoto University,
Sakyo-ku,
Kyoto, Japan

Introduction

Neuroendocrine tumours (NETs) represent a large group of neoplasms derived from pluripotent stem cells or from differentiated neuroendocrine cells that are characterised by the expression of various peptides and biogenic amines [1]. NETs are capable of causing severe disease due to the excessive secretion of a variety of hormones. Surgical resection and debulking offer the best palliation for those affected, but treatment is rarely curative owing to the extent of the disease [2–4].

Meta-iodobenzylguanidine (MIBG) is an alkyl-guanidine derivative that is similar to noradrenaline and is accumulated by tissue arising from adrenal medullary tumours and many other NETs [5, 6]. Therefore, it has been expected that radionuclide therapy with ^{131}I-labelled meta-iodobenzylguanidine ([^{131}I]MIBG) will be effective for the treatment of NETs [7–10].

On the other hand, P-glycoprotein (P-gp) has been reported to be expressed in some types of NET [11–14]. P-gp can transport a wide range of structurally unrelated,

lipophilic, neutral and cationic organic compounds [15, 16] and produces multidrug resistance in cells [15, 16]. Since MIBG is a lipophilic and cationic compound, it has the potential to be a substrate of P-gp. Thus, if MIBG were a substrate of P-gp, the therapeutic effect of [^{131}I]MIBG for NETs would vary according to P-gp expression and the dose of [^{131}I]MIBG would be affected by tumour characteristics.

Therefore, in this study, using a porcine kidney cell line which overexpresses human P-gp, LLC-GA5-COL150 [17], we investigated whether MIBG is a substrate of P-gp.

Materials and methods

General

[^{3}H]daunomycin (592 GBq/mmol) and D-[^{14}C]mannitol (1987 MBq/mmol) were purchased from PerkinElmer Life Sciences (Boston, MA). [^{125}I]MIBG (1.80 TBq/mmol) was kindly supplied by Daiichi Radioisotope Laboratories (Tokyo, Japan). All chemicals used in this study were of the highest purity available.

Cell lines and cell culture

LLC-GA5-COL150 cells were established to be transfected with human MDR1 cDNA into porcine kidney cells, LLC-PK$_1$ [17]. LLC-GA5-COL150 cells overexpress human P-gp on the apical membrane. LLC-PK$_1$ cells were used as host cells without P-gp. Complete medium consisted of Dulbecco's modified Eagle's medium supplemented with 10% fetal bovine serum without antibiotics, and 150 ng/ml colchicine was added to the medium for LLC-GA5-COL150 cells. Monolayers were grown under an atmosphere of 5% CO_2/95% air at 37°C, and were subcultured every 6–7 days using 0.02% EDTA and 0.05% trypsin. For the transport studies, LLC-GA5-COL150 and LLC-PK$_1$ cells were seeded on polycarbonate membrane filters (3-μm pores, 4.71 cm^2 growth area) inside Transwell cell culture chambers (Coaster, Cambridge, MA) at a density of 5×10^5 and 4×10^5 cells/cm^2, respectively. Transwell chambers were placed in 35-mm wells of tissue culture plates with 2.6 ml of medium outside (basolateral side) and 1.5 ml inside (apical side). Medium was replaced every 2 days, and the cells were used on the 7th day after seeding.

Immunoblot analysis

Cells were homogenised in PBS containing 1% Nonidet P40, 0.5% deoxycholic acid sodium salt and 0.1% SDS. The homogenate was subjected to SDS-PAGE (5–20% gradient gel). The separated proteins were electrophoretically transferred onto a polyvinylidine difluoride membrane (Millipore, Billerica, MO). Primary and secondary antibodies were commercially obtained and used: anti-P-gp antibody (1:500, Calbiochem, Darmstadt, Germany) and horseradish peroxidase-conjugated anti-mouse IgG2a antibody (1:10,000, Santa Cruz biotechnology, Santa Cruz, CA). The membrane was stained using ECL kit (Amersham Biosciences) according to the manufacturer's instructions.

Transport and cellular accumulation measurements

Transport and cellular accumulation measurements were performed as described previously with some modifications [17, 18]. Figure 1 shows a schematic diagram of the

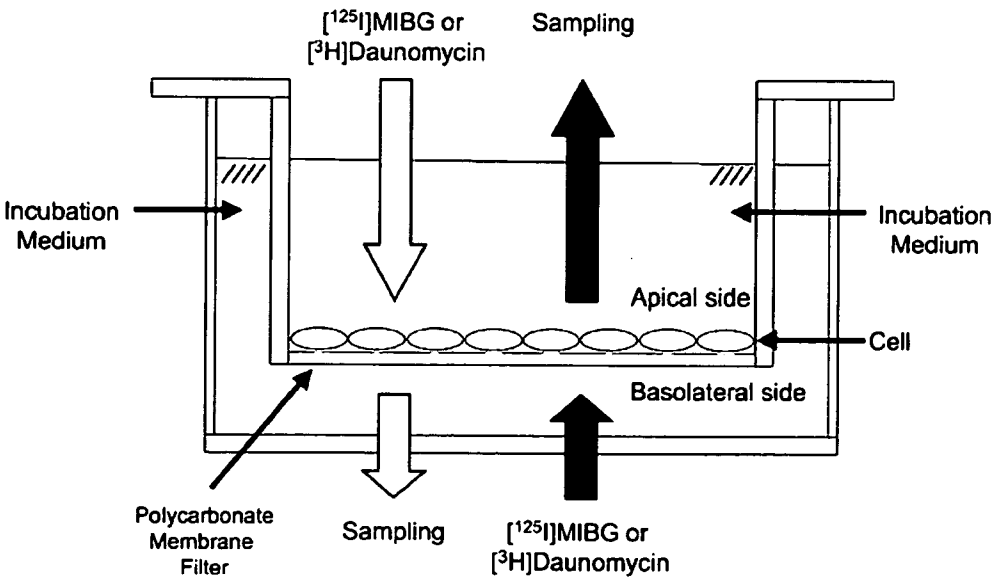

Fig. 1 Schematic diagram of the transcellular transport experiment. [^{125}I]MIBG and [^{3}H] daunomycin were added to either the basolateral or the apical side, aliquots of the incubation medium on the other side were taken at specified times, and the radioactivity was measured

transcellular transport experiments. The transcellular transport and accumulation of [^{3}H]daunomycin and [^{125}I]MIBG were measured using monolayer cultures grown in Transwell chambers. The composition of the incubation medium was as follows: 145 m*M* NaCl, 3 m*M* KCl, 1 m*M* $CaCl_2$, 0.5 m*M* $MgCl_2$, 5 m*M* D-glucose and 5 m*M* HEPES (pH 7.4). Six hours before the transport experiments, the culture medium was replaced with fresh colchicine-free culture medium. After removal of the culture medium from both sides of the monolayers, the cell monolayers were preincubated with 2 ml of incubation medium in each side for 15 min at 37°C. Then, 2 ml of incubation medium containing radioactive substrate was added to either the basolateral or the apical side, 2 ml of nonradioactive incubation medium was added to the opposite side, and the monolayers were incubated for specified periods at 37°C. D-[^{14}C]mannitol (2 m*M*, 3.6 kBq/ml), a compound that is not transported by cells, was used to calculate the paracellular fluxes and the extracellular trapping of [^{3}H] daunomycin and [^{125}I]MIBG. For transport measurements, aliquots (50 µl) of the incubation medium on the other side were taken at specified times, and the radioactivity was measured.

For accumulation experiments, the medium was removed by aspiration at the end of the incubation period, and the monolayers were rapidly washed twice with 2 ml of ice-cold incubation medium on each side. The filters with the monolayers were detached from the chambers, the cells on the filters were solubilised with 0.5 ml of 1 *N* NaOH, and the radioactivity in aliquots of 50 µl was measured. The radioactivity of the collected medium and the solubilised cell monolayers was determined in 3 ml of ACS II (Amersham, Buckinghamshire, UK) by liquid scintillation counting. The protein contents of the monolayers solubilised in 1 *N* NaOH were determined by the BCA method using a BCA protein assay kit (Pierce, Rockford, IL) with BSA as a standard.

Statistical analysis

Statistical analyses were performed with an unpaired *t* test. Differences were considered significant when $p<0.05$.

Results

Immunoblot analysis

Immunoblot analysis was performed to examine the expression of P-gp in LLC-PK_1 and LLC-GA5-COL150 cells (Fig. 2). P-gp was detected clearly at 170 kDa in LLC-GA5-COL150 cells, although it was not detected in LLC-PK_1 cells.

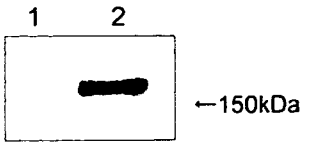

Fig. 2 Immunoblot analysis of homogenate from LLC-PK_1 (*lane 1*) and LLC-GA5-COL150 (*lane 2*)

Transcellular transport and accumulation of daunomycin

First, to confirm the validity of our experimental system using LLC-GA5-COL150 monolayers for evaluation of transportation by P-gp, we measured the transcellular transport and cellular accumulation of daunomycin (100 n*M*) by LLC-GA5-COL150 cells, compared with LLC-PK_1 cells, which do not express P-gp (Fig. 3). In LLC-PK_1 cells, there was no significant difference between the apical-to-basolateral transport and the basolateral-to-apical transport of daunomycin. In contrast, the basolateral-to-apical transport rate of daunomycin by LLC-GA5-COL150 monolayers was higher than that in the opposite direction. Furthermore, the basolateral-to-apical transport of daunomycin was significantly increased in LLC-GA5-COL150 monolayers compared with that in LLC-PK_1 monolayers ($p<0.01$, Fig. 3a). The cellular accumulation of daunomycin in both directions was significantly lower in LLC-GA5-COL150 than in LLC-PK_1 ($p<0.01$, Fig. 3b).

Transcellular transport and accumulation of MIBG

The transcellular transport of MIBG (100 n*M*) was examined using the LLC-GA5-COL150 and LLC-PK_1 monolayers. There were no significant differences in the transport of MIBG between LLC-GA5-COL150 and LLC-PK_1 monolayers in either direction until 60 min (Fig. 4a). As regards the accumulation of MIBG, again there were no significant differences between LLC-GA5-COL150 and LLC-PK_1 cells in either direction (Fig. 4b). Furthermore, the basolateral-to-apical transport of MIBG was much greater than the apical-to-basolateral transport in both LLC-GA5-COL150 and LLC-PK_1 monolayers (Fig. 4a). The patterns of transport and accumulation of MIBG were obviously different from those of daunomycin.

Discussion

Most substrates for P-gp are extensively transported by LLC-GA5-COL150 compared with LLC-PK_1 monolayers, accompanied by a decrease in intracellular accumulation. In our system, the basolateral-to-apical transport of daunomycin was significantly increased in LLC-GA5-COL150 compared with LLC-PK_1 monolayers, but there was no significant difference between LLC-GA5-COL150 and

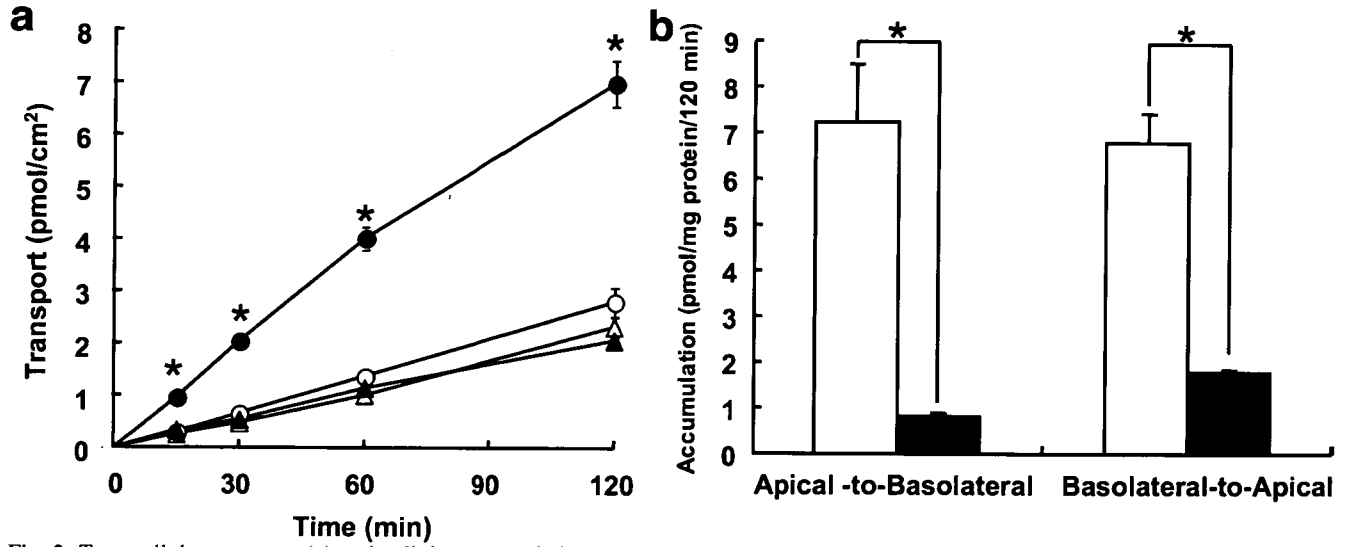

Fig. 3 Transcellular transport (**a**) and cellular accumulation (**b**) of daunomycin by LLC-GA5-COL150 and LLC-PK$_1$ monolayers. LLC-GA5-COL150 (*solid symbols*) and LLC-PK$_1$ (*open symbols*) monolayers were incubated at 37°C with 100 n*M* [^{3}H]daunomycin added to either the apical (*triangles*) or the basolateral (*circles*) side of the monolayers. After incubation, the appearance of radioactivity on the opposite side and accumulation were measured. Each point represents the mean±SEM of three independent experiments. *$p<0.01$, significant difference from LLC-PK$_1$ monolayers

LLC-PK$_1$ monolayers in the apical-to-basolateral transport of daunomycin (Fig. 3a). In addition, the accumulation of daunomycin in LLC-GA5-COL150 monolayers was significantly decreased compared with that in LLC-PK$_1$ monolayers on both sides (Fig. 3b). If there is no specific transport system for daunomycin, the apical-to-basolateral and reverse transport rates should be same. However, because human P-gp localises specifically in the apical membrane of LLC-GA5-COL150 cells, substrates for P-gp coming from apical side are likely to be caught and pumped back out to the medium, resulting in a reduced apical-to-basolateral transport rate. By contrast, substrates entering cells from basolateral side will be discharged across the apical membranes, resulting in acceleration of the basolateral-to-apical transport rate. Furthermore, decreased accumulation of P-gp substrates in LLC-GA5-COL150 cells is due to expulsion of substrates across the apical membranes via P-gp. These results demonstrate that our system using LLC-GA5-COL150 cells is suitable for evaluation of the transport of a compound by P-gp.

The basolateral-to-apical transport of MIBG was significantly greater than the apical-to-basolateral transport in both monolayers (Fig. 4a). Furthermore, there was no significant difference between LLC-GA5-COL150 and

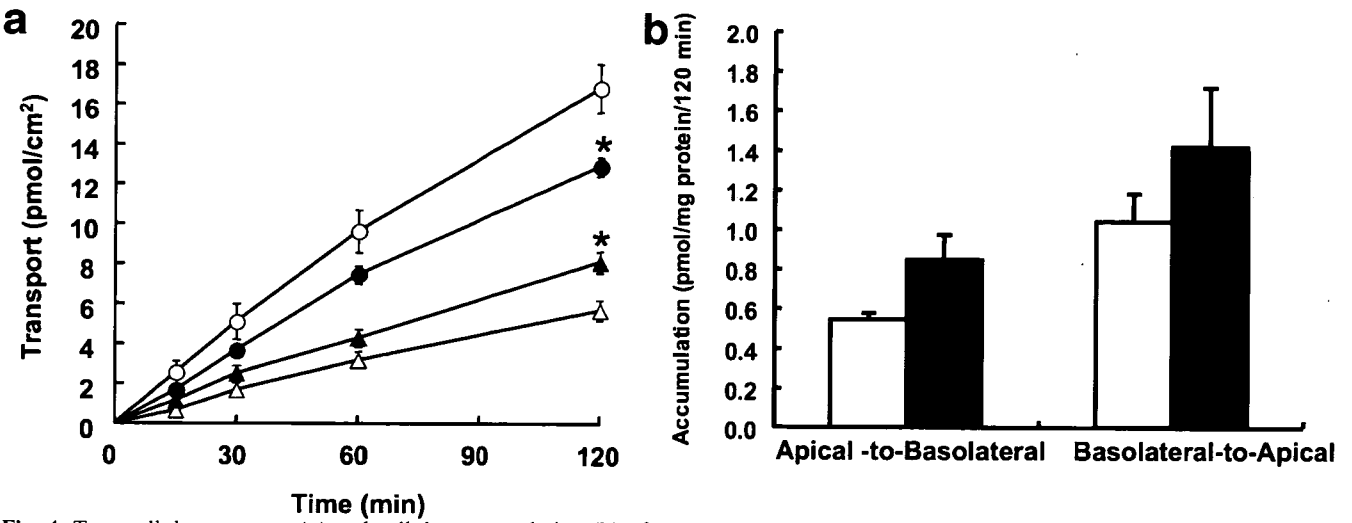

Fig. 4 Transcellular transport (**a**) and cellular accumulation (**b**) of MIBG by LLC-GA5-COL150 and LLC-PK$_1$ monolayers. LLC-GA5-COL150 (*solid symbols*) and LLC-PK$_1$ (*open symbols*) monolayers were incubated at 37°C with 100 n*M* [^{125}I]MIBG added to either the apical (triangles) or the basolateral (*circles*) side of monolayers. Each point represents the mean±SEM of three independent experiments. *$p<0.05$, significant difference from LLC-PK$_1$ monolayers

LLC-PK_1 monolayers in either direction (Fig. 4b). These transport and accumulation patterns are obviously different from those obtained in respect of daunomycin. Therefore, these results indicate that MIBG is not a substrate of P-gp.

The patterns of transport and accumulation also suggest that MIBG is subjected to directional transport across LLC-PK_1 monolayers. In LLC-PK_1 cells, there are organic cation transporters (OCTs) [19–22]. Since, under physiological conditions, MIBG has a cationic charge at the guanidino group, there is a possibility that it is transported by OCTs. In fact, cimetidine, an inhibitor of OCTs, inhibited both the apical-to-basolateral and the basolateral-to-apical transport of MIBG (data not shown). In addition to OCTs, the multidrug resistance-related protein family and/or the Bcl protein family may also transport MIBG. More studies are required on the possible transport of MIBG by many transporters.

In conclusion, MIBG is not a substrate of P-gp. Therefore, radionuclide therapy with MIBG would be useful in the treatment of NETs even if the tumour cells express P-gp.

Acknowledgements We would like to thank Daiichi Radioisotope Laboratories Ltd., Tokyo, Japan, for providing [^{125}I]MIBG. This study was supported in part by Grants-in-aid for General Scientific Research from the Ministry of Education, Culture, Sports, and Science.

References

1. Bombardieri E, Seregni E, Villano C, Chiti A, Bajetta E. Position of nuclear medicine techniques in the diagnostic work-up of neuroendocrine tumors. Q J Nucl Med Mol Imaging 2004;48:150–3.
2. Chamberlain RS, Canes D, Brown KT, Saltz L, Jarnagin W, Fong Y, et al. Hepatic neuroendocrine metastases: does intervention alter outcomes? J Am Coll Surg 2000;190:432–5.
3. Carty SE, Jensen RT, Norton JA. Prospective study of aggressive resection of metastatic pancreatic endocrine tumors. Surgery 1992;112:1024–31; discussion 1031–2.
4. Norton JA, Warren RS, Kelly MG, Zuraek MB, Jensen RT. Aggressive surgery for metastatic liver neuroendocrine tumors. Surgery 2003;134:1057–3; discussion 1063–5.
5. Wieland DM, Wu J, Brown LE, Mangner TJ, Swanson DP, Beierwaltes WH. Radiolabeled adrenergi neuron-blocking agents: adrenomedullary imaging with [^{131}I]iodobenzylguanidine. J Nucl Med 1980;21:349–53.
6. Wafelman AR, Hoefnagel CA, Maes RA, Beijnen JH. Radioiodinated metaiodobenzylguanidine: a review of its biodistribution and pharmacokinetics, drug interactions, cytotoxicity and dosimetry. Eur J Nucl Med 1994;21:545–59.
7. Mukherjee JJ, Kaltsas GA, Islam N, Plowman PN, Foley R, Hikmat J, et al. Treatment of metastatic carcinoid tumours, phaeochromocytoma, paraganglioma and medullary carcinoma of the thyroid with ^{131}I-meta-iodobenzylguanidine [^{131}I-mIBG]. Clin Endocrinol (Oxf) 2001;55:47–60.
8. Safford SD, Coleman RE, Gockerman JP, Moore J, Feldman JM, Leight GS Jr, et al. Iodine -131 metaiodobenzylguanidine is an effective treatment for malignant pheochromocytoma and paraganglioma. Surgery 2003;134:956–62; discussion 962–3.
9. Bomanji JB, Wong W, Gaze MN, Cassoni A, Waddington W, Solano J, et al. Treatment of neuroendocrine tumours in adults with ^{131}I-MIBG therapy. Clin Oncol (R Coll Radiol) 2003;15:193–8.
10. Safford SD, Coleman RE, Gockerman JP, Moore J, Feldman J, Onaitis MW, et al. Iodine-131 metaiodobenzylguanidine treatment for metastatic carcinoid. Results in 98 patients. Cancer 2004;101:1987–93.
11. Campling BG, Young LC, Baer KA, Lam YM, Deeley RG, Cole SP, et al. Expression of the MRP and MDR1 multidrug resistance genes in small cell lung cancer. Clin Cancer Res 1997;3:115–22.
12. Chan HS, Haddad G, Thorner PS, DeBoer G, Lin YP, Ondrusek N, et al. P-glycoprotein expression as a predictor of the outcome of therapy for neuroblastoma. N Engl J Med 1991;325:1608–14.
13. De Moerloose B, Van de Wiele C, Dhooge C, Philippe J, Speleman F, Benoit Y, et al. Technetium-99m sestamibi imaging in paediatric neuroblastoma and ganglioneuroma and its relation to P-glycoprotein. Eur J Nucl Med 1999;26:396–403.
14. Goldstein LJ, Galski H, Fojo A, Willingham M, Lai SL, Gazdar A, et al. Expression of a multidrug resistance gene in human cancers. J Natl Cancer Inst 1989;81:116–24.
15. Gottesman MM, Fojo T, Bates SE. Multidrug resistance in cancer: role of ATP-dependent transporters. Nat Rev Cancer 2002;2:48–58.
16. Ambudkar SV, Kimchi-Sarfaty C, Sauna ZE, Gottesman MM. P-glycoprotein: from genomics to mechanism. Oncogene 2003;22:7468–85.
17. Tanigawara Y, Okamura N, Hirai M, Yasuhara M, Ueda K, Kioka N, et al. Transport of digoxin by human P-glycoprotein expressed in a porcine kidney epithelial cell line (LLC-PK_1). J Pharmacol Exp Ther 1992;263:840–5.
18. Soares-Da-Silva P, Serrao MP. Outward transfer of dopamine precursor L-3,4-dihydroxyphenylalanine (L-dopa) by native and human P-glycoprotein in LLC-PK_1 and LLC-GA5 col300 renal cells. J Pharmacol Exp Ther 2000;293:697–704.
19. Saito H, Yamamoto M, Inui K, Hori R. Transcellular transport of organic cation across monolayers of kidney epithelial cell line LLC-PK. Am J Physiol 1992;262:C59–66.
20. Ohtomo T, Saito H, Inotsume N, Yasuhara M, Inui KI. Transport of levofloxacin in a kidney epithelial cell line, LLC-PK_1: interaction with organic cation transporters in apical and basolateral membranes. J Pharmacol Exp Ther 1996;276:1143–8.
21. Takami K, Saito H, Okuda M, Takano M, Inui KI. Distinct characteristics of transcellular transport between nicotine and tetraethylammonium in LLC-PK_1 cells. J Pharmacol Exp Ther 1998;286:676–80.
22. Urakami Y, Kimura N, Okuda M, Masuda S, Katsura T, Inui K. Transcellular transport of creatinine in renal tubular epithelial cell line LLC-PK_1. Drug Metab Pharmacokinet 2005;20:200–5.

Synthesis and evaluation of radioiodinated (*S,S*)-2-(α-(2-iodophenoxy)benzyl)morpholine for imaging brain norepinephrine transporter

Naoki Kanegawa[1], Yasushi Kiyono[2], Hiroyuki Kimura[1], Taku Sugita[1], Satomi Kajiyama[1], Hidekazu Kawashima[3], Masashi Ueda[4], Yuji Kuge[1], Hideo Saji[1]

[1] Department of Patho-Functional Bioanalysis, Graduate School of Pharmaceutical Sciences, Kyoto University, Sakyo-ku, Kyoto, 606-8501, Japan
[2] Radioisotopes Research Laboratory, Kyoto University Hospital, Faculty of Medicine, Kyoto University, Sakyo-ku, Kyoto, Japan
[3] Department of Nuclear Medicine and Diagnostic Imaging, Graduate School of Medicine, Kyoto University, Sakyo-ku, Kyoto, Japan
[4] Radioisotope Laboratory, Kyoto Prefectural University of Medicine, Sakyo-ku, Kyoto, Japan

Received: 24 August 2005 / Accepted: 28 September 2005 / Published online: 8 March 2006

Abstract. *Purpose:* Abnormality of the brain norepinephrine transporter (NET) has been reported in several psychiatric and neuronal disorders. Since NET is an important target for the diagnosis of these diseases, the development of radiopharmaceuticals for imaging of brain NET has been eagerly awaited. In this study, we synthesized (*S,S*)-2-(α-(2-iodophenoxy)benzyl)morpholine [(S,S)-IPBM], a derivative of reboxetine iodinated at position 2 of the phenoxy ring, and evaluated its potential as a radiopharmaceutical for imaging brain NET using SPECT.
Methods: (S,S)-$^{123/125}$I-IPBM was synthesized in a halogen exchange reaction. The affinity and selectivity of (S,S)-IPBM for NET was measured by assaying the displacement of ^{3}H-nisoxetine and (S,S)-^{125}I-IPBM from the binding site in rat brain membrane, respectively. The biodistribution of (S,S)-^{125}I-IPBM was also determined in rats. Furthermore, SPECT studies with (S,S)-^{123}I-IPBM were carried out in the common marmoset.
Results: (S,S)-^{125}I-IPBM was prepared with high radiochemical yields (65%) and high radiochemical purity (>98%). (S,S)-IPBM showed high affinity and selectivity for NET in the binding assay experiments. In biodistribution experiments, (S,S)-^{125}I-IPBM showed rapid uptake in the brain, and the regional cerebral distribution was consistent with the density of NET. The administration of nisoxetine, a selective NET-binding agent, decreased the accumulation of (S,S)-^{125}I-IPBM in the brain, but the administration of selective serotonin transporter and dopamine transporter binding agents caused no significant changes in the accumulation. Moreover, (S,S)-^{123}I-IPBM allowed brain NET imaging in the common marmoset with SPECT.
Conclusion: These results suggest that (S,S)-^{123}I-IPBM is a potential SPECT radiopharmaceutical for imaging brain NET.

Keywords: Norepinephrine transporter – Radioiodination – Brain – SPECT – (*S,S*)-2-(a-(2-iodo-phenoxy)benzyl) morpholine

Eur J Nucl Med Mol Imaging (2006) 33:639–647
DOI 10.1007/s00259-005-0017-y

Introduction

The norepinephrine transporter (NET), which is located in the presynaptic terminal of noradrenergic neurons, plays a critical role in the norepinephrine (NE) reuptake system and regulates the synaptic NE concentration [1, 2]. Since decreased levels of NET have been reported to be related to various diseases of the brain, including depression β–5] and Alzheimer's disease [6, 7], NET could be an important target for the diagnosis of these diseases. Therefore, a NET-specific radioligand is expected to be developed for assessment of changes in NET density in various brain disorders in vivo.

A radioiodine-substituted analog of the potent NET-binding agent nisoxetine, radioiodinated (R)-MIPP, was developed as a radiopharmaceutical for brain NET imaging [8, 9]. Although (R)-^{125}I-MIPP had high affinity for NET, it also had moderate affinity for the serotonin transporter (SERT) [8, 10, 11]. Therefore, (R)-^{125}I-MIPP lacked selectivity for NET in vivo.

Hideo Saji (✉)
Department of Patho-Functional Bioanalysis,
Graduate School of Pharmaceutical Sciences,
Kyoto University,
Sakyo-ku, Kyoto 606-8501, Japan
e-mail: hsaji@pharm.kyoto-u.ac.jp
Tel.: +81-75-7534556, Fax: +81-75-7534568

Recently, reboxetine has been reported to be a highly selective NET-binding agent, with about 400-fold selectivity favoring norepinephrine reuptake inhibition over serotonin reuptake inhibition [12]. Wilson et al. reported the promising compound ^{11}C-labeled *O*-methyl reboxetine, (S,S)-^{11}C-MeNER, for the imaging of brain NET in vivo with positron emission tomography (PET) [13]. Although (S,S)-^{11}C-MeNER showed specific binding to NET, it caused problems in quantitative studies owing to the short half-life of ^{11}C (20 min, in that it did not reach a specific binding peak equilibrium during the PET measurements [14, 15]. ^{123}I has a half-life of 13.3 h, which is ideal for the slower kinetics of reboxetine analogs. Therefore, the superior radiation properties of ^{123}I for SPECT prompted us to develop a radioiodinated ligand for imaging of brain NET.

We expected the introduction of iodine at position 2 of the phenoxy ring not to affect the affinity and selectivity for NET, because a reboxetine analog substituted at this position has been reported to have high affinity and selectivity for NET [13, 16]. Thus, we designed (*S,S*)-2-(α-(2-iodophenoxy)benzyl)morpholin [(S,S)-IPBM] iodinated at position 2 of the phenoxy ring as a radiopharmaceutical for imaging brain NET in vivo (Fig. 1). In this study, radioiodinated (S,S)-IPBM was synthesized and its potential as an imaging agent assessed.

Materials and methods

General

Sodium ^{125}I-iodide (643.8 GBq/mg) and ^{3}H-nisoxetine (2.96 TBq/mmol) were purchased from New England Nuclear (Boston, MA). Sodium ^{123}I-iodide (1.48 GBq/ml) was kindly provided by Daiichi Radioisotope Laboratories (Tokyo, Japan). All chemicals used in this study were of reagent grade.

Proton nuclear magnetic resonance (^{1}H-NMR) spectra were recorded on a JNM-AL 400 spectrometer (JEOL Ltd. Tokyo, Japan), and the chemical shifts were reported in parts per million (ppm) downfield from an internal tetramethylsilane standard. Electrospray ionization mass spectra were recorded with a LC-MS QP8000α (Shimadzu Ltd. Kyoto, Japan). The optical rotation of compounds was measured with a SEPA-200 spectrometer (Horiba Ltd. Kyoto, Japan).

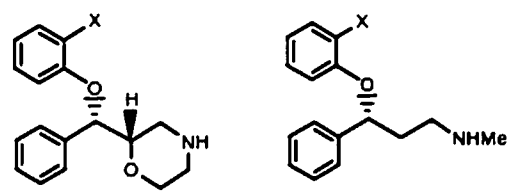

Fig. 1. Chemical structures of reboxetine analogs

Animal studies were conducted in accordance with our institutional guidelines, and the experimental procedures were approved by the Kyoto University Animal Care Committee.

Synthesis

Synthesis of (R,R)/(S,S)-IPBM

The synthetic pathway is shown in Fig. 2. (S,S)-IPBM was synthesized referring to the synthetic procedure of reboxetine outlined by Melloni et al. [17].

(2R,3S)/(2S,3R)-1,2-dihydroxy-3-(2-iodophenoxy)-3-phenyl-propane (3a) ^{1}H-NMR ($CDCl_3$) δ 3.78 (1H, m, -CH-C$\underline{H}_A$H$_B$-OH), 3.97 (1H, m, -CH-CH$_A\underline{H}_B$-OH), 4.02 (1H, m, -C$\underline{H}$-OH), 5.38 (1H, d, Ph-C$\underline{H}$, J = 4.6 Hz), 6.58–7.75 (4H, m, $\underline{Ph}$-O), 7.39 (5H, m, $\underline{Ph}$-C). ESI-MS calcd for $C_{15}H_{15}O_3INa$ $[M + Na]^+$: m/z 393, found 393.

(2R,3S)/(2S,3R)-2-hydroxy-3-(2-iodophenoxy)-1-(4-nitro-benzoyloxy)-3-phenylpropane (4a) ^{1}H-NMR ($CDCl_3$) δ 2.56 (1H, d, O$\underline{H}$), 4.40 (1H, m, -C$\underline{H}$-OH), 4.65 (1H, m, C$\underline{H}_A$H$_B$OCO), 4.73 (1H, m, CH$_A\underline{H}_B$OCO), 5.37 (1H, d, Ph-C$\underline{H}$, J = 5.1 Hz), 6.69–7.77 (4H, m,

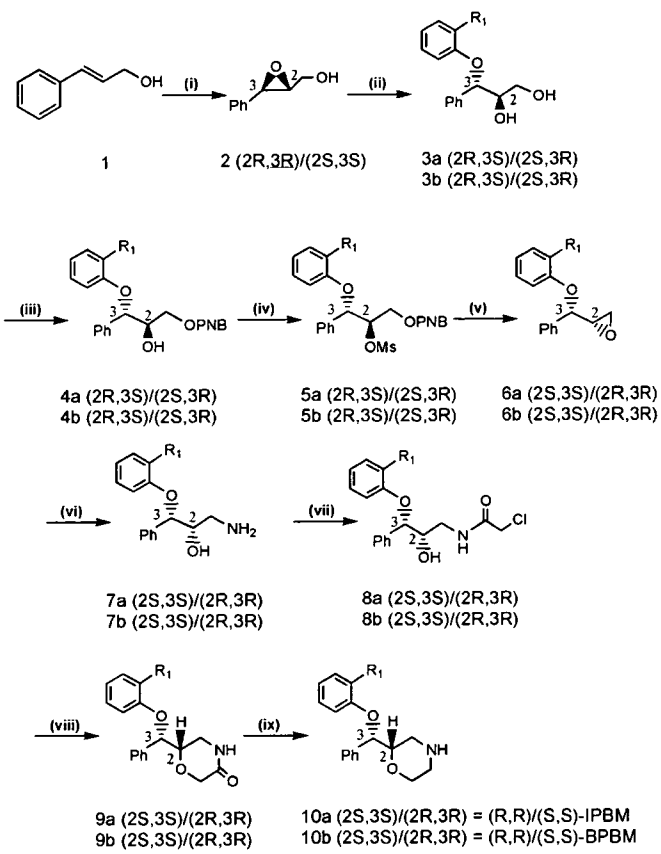

Fig. 2. Synthesis of halogenated reboxetine analogs. *a*, (R,R)/(S,S)-IPBM (R_1=I); *b*, (R,R)/(S,S)-BPBM (R_1=Br). Reagents: (i) mCPBA, CH_2Cl_2; (ii) 2-halogenated phenol, aq.NaOH; (iii) pyridine, PNBCl; (iv) MsCl, Et_3N, $CHCl_3$; (v) aq.NaOH, dioxane; (vi) NH_4OH, MeOH; (vii) $ClCOCH_2Cl$, TEA, $CHCl_3$; (viii) KO*t*Bu, *t*-BuOH; (ix) BH_3, THF. Only one optical isomer is shown in the scheme, that which is underlined, for the sake of clarity

Ph-O), 7.37 (5H, m, Ph-C), 8.12–8.24 (4H, m, Ph-N). ESI-MS calcd for $C_{22}H_{19}NO_6I$ $[M + H]^+$: m/z 520, found 520. Anal. calcd for $C_{22}H_{18}NO_6I$: C, 50.88; H, 3.49; N, 2.70; O, 18.49%; Found: C, 50.84; H, 3.49; N, 2.51; O, 18.72%.

(2R,3S)/(2S,3R)-3-(2-iodophenoxy)-2-mesyloxy-1-(4-nitro-benzoyloxy)-3-phenylpropane (5a) ^{1}H-NMR ($CDCl_3$) δ 2.67 (3H, s, CH_3S), 4.93 (2H, m, $-CH_2-OCO$), 5.34 (1H, m, $CHOSO_2$), 5.53 (1H, d, Ph-CH, J = 5.4 Hz), 6.59–7.78 (4H, m, Ph-O), 7.43 (5H, m, Ph-C), 8.19–8.26 (4H, m, Ph-N). ESI-MS calcd for $C_{23}H_{21}NO_8SI$ $[M + H]^+$: m/z 598, found 598.

(2S,3S)/(2R,3R)-3-(2-iodophenoxy)-3-phenylpropene-1,2-epoxide (6a) A solution of crude 5a (2.93 g, 4.90 mmol) in dioxane (29.3 ml) and 1 *N* NaOH (16 ml) was stirred for 4 h at room temperature. After being diluted with water, the solution was extracted with ethyl acetate. The organic phase was washed with a saturated solution of $NaHCO_3$ and brine and evaporated to dryness. Purification of the crude product by chromatography on silica gel (hexane:ethyl acetate=10:1) gave pure 6a as a colorless oil. The yield was 1.22 g (70%). ^{1}H-NMR ($CDCl_3$) δ 2.82 (2H, m, CH_2-CH), 3.47 (1H, m, CH_2-CH), 4.98 (1H, d, -Ph-CH, J = 5.9 Hz), 6.68–7.76 (4H, m, Ph-O), 7.40 (5H, m, Ph-C). ESI-MS calcd for $C_{15}H_{13}O_2INa$ $[M + Na]^+$: m/z 375, found 375.

(2S,3S)/(2R,3R)-1-amino-2-hydroxy-3-(2-iodophenoxy)-3-phenylpropane (7a) ^{1}H-NMR, free base ($CDCl_3$) δ 2.73 (1H, m, CH_AH_BN), 2.84 (1H, m, CH_AH_BN), 3.96 (1H, m, CH-OH), 5.16 (1H, d, Ph-CH, J = 6.8 Hz), 6.60–7.73 (4H, m, Ph-O), 7.35 (5H, m, Ph-C). ESI-MS calcd for $C_{15}H_{17}NO_2I$ $[M + H]^+$: m/z 370, found 370.

(2S,3S)/(2R,3R)-1-chloroacetylamino-2-hydroxy-3-(2-iodo-phenoxy)-3-phenylpropane (8a) ^{1}H-NMR ($CDCl_3$) δ 3.39 (1H, m, CH_AH_BN), 3.50 (1H, m, CH_AH_BN), 4.03 (2H, q, CH_2-Cl), 4.13 (1H, m, CH-OH), 5.03 (1H, d, Ph-CH, J = 6.8 Hz), 6.58–7.74 (4H, m, Ph-O), 6.99 (1H, brs, NH), 7.35 (5H, m, Ph-C). ESI-MS calcd for $C_{17}H_{17}NO_3ClINa$ $[M + Na]^+$: m/z 468, found 468.

(2S,3S)/(2R,3R)-2-[α-(2-iodophenoxy)benzyl]morpholine-5-one (9a) ^{1}H-NMR ($CDCl_3$) δ 3.26 (1H, m, CH_AH_BN), 3.35 (1H, m, CH_AH_BN), 4.26 (1H, m, O-CH-CH-Ph), 4.31 (2H, q, CH_2CO), 5.36 (1H, d, Ph-CH, J = 5.9 Hz), 5.84 (1H, brs, CONH), 6.65–7.75 (4H, m, Ph-O), 7.35 (5H, m, Ph-C). ESI-MS calcd for $C_{17}H_{17}NO_3I$ $[M + H]^+$: m/z 410, found 410. Anal. calcd for $C_{17}H_{16}NO_3I$: C, 49.90; H, 3.94; N, 3.42%; Found: C, 49.47; H, 3.94; N, 3.31%.

(2S,3S)/(2R,3R)-2-[α-(2-iodophenoxy)benzyl]morpholine (10a) ^{1}H-NMR ($CDCl_3$) δ 2.61 (1H, m, O-CH_AH_BN), 2.80 (3H, m, O-CH_AH_BN-CH_2-), 3.66 (1H, m, O-CH-CH-Ph), 3.96 (2H, m, CH_2CO), 5.21 (1H, d, Ph-CH, J = 5.6 Hz), 6.63–7.72 (4H, m, Ph-O), 7.34 (5H, m, Ph-C). ESI-MS calcd for $C_{17}H_{19}NO_2I$ $[M + H]^+$: m/z 396, found 396. Anal. Calcd for $C_{17}H_{18}NO_2I$: C, 51.66; H, 4.59; N, 3.54%; Found: C, 51.56; H, 4.56; N, 3.45%.

Synthesis of (R,R)/(S,S)-BPBM

(S,S)-BPBM was synthesized in the same manner as (S,S)-IPBM, using 2-bromophenol as a starting material instead of 2-iodophenol.

(2R,3S)/(2S,3R)-1,2-dihydroxy-3-(2-bromophenoxy)-3-phenylpropane (3b) ^{1}H-NMR ($CDCl_3$) δ 3.76 (1H, m, -CH-CH_AH_B-OH), 3.95 (1H, m, -CH-CH_AH_B-OH), 4.02 (1H, m, -CH-OH), 5.38 (1H, d, Ph-CH, J = 4.6 Hz), 6.65–7.52 (4H, m, Ph-O), 7.34 (5H, m, Ph-C).

(2R,3S)/(2S,3R)-2-hydroxy-3-(2-bromophenoxy)-1-(4-nitro-benzoyloxy)-3-phenylpropane (4b) ^{1}H-NMR ($CDCl_3$) δ 4.40 (1H, m, -CH-OH), 4.67 (2H, m, CH_2OCO), 5.35 (1H, d, Ph-CH, J = 5.1 Hz), 6.67–7.54 (4H, m, Ph-O), 7.38 (5H, m, Ph-C), 8.12–8.25 (4H, m, Ph-N). ESI-MS calcd for $C_{22}H_{19}NO_6Br$ $[M + H]^+$: m/z 472, found 472.

(2R,3S)/(2S,3R)-3-(2-bromophenoxy)-2-mesyloxy-1-(4-nitro-benzoyloxy)-3-phenylpropane (5b) ^{1}H-NMR ($CDCl_3$) δ 2.68 (3H, s, CH_3S), 4.80 (1H, m, -CH_AH_B-OCO), 4.94 (1H, m, -CH_AH_B-OCO), 5.36 (1H, m, $CHOSO_2$), 5.50 (1H, d, Ph-CH, J = 5.2 Hz), 6.68–7.54 (4H, m, Ph-O), 7.44 (5H, m, Ph-C), 8.20–8.26 (4H, m, Ph-N).

(2S,3S)/(2R,3R)-3-(2-bromophenoxy)-3-phenylpropene-1,2-epoxide (6b) ^{1}H-NMR ($CDCl_3$) δ 2.80 (1H, m, CH_AH_B-CH), 2.85 (1H, m, CH_AH_B -CH), 3.47 (1H, m, CH_2-CH), 4.97 (1H, d, -Ph-CH, J = 5.9 Hz), 6.79–7.54 (4H, m, Ph-O), 7.42 (5H, m, Ph-C). ESI-MS calcd for $C_{15}H_{13}O_2BrNa$ $[M + Na]^+$: m/z 327, found 327.

(2S,3S)/(2R,3R)-1-amino-3-(2-bromophenoxy)-2-hydroxy-3-phenylpropane (7b) ^{1}H-NMR, free base, ($CDCl_3$) δ 2.71 (2H, m, CH_AH_BN), 2.80 (2H, m, CH_AH_BN), 3.96 (1H, m, CH-OH), 5.14 (1H, d, Ph-CH, J = 6.8 Hz), 6.69–7.51 (4H, m, Ph-O), 7.36 (5H, Ph-C). ESI-MS calcd for $C_{15}H_{17}NO_2Br$ $[M + H]^+$: m/z 322, found 322.

(2S,3S)/(2R,3R)-3-(2-bromophenoxy)-1-chloroacetylamino-2-hydroxy-3-phenylpropane (8b) ^{1}H-NMR ($CDCl_3$) δ 3.39 (1H, m, CH_AH_BN), 3.48 (1H, m, CH_AH_BN), 4.03 (2H, q, CH_2-Cl), 4.14 (1H, m, CH-OH), 5.00 (1H, d, Ph-CH, J = 6.8 Hz), 6.66–7.52 (4H, m, Ph-O), 7.03 (1H, brs, NH), 7.37 (5H, m, Ph-C). ESI-MS calcd for $C_{17}H_{17}NO_3ClBrNa$ $[M + Na]^+$: m/z 420, found 420.

(2S,3S)/(2R,3R)-2-[α-(2-bromophenoxy)benzyl]morpholine-5-one (9b) ^{1}H-NMR ($CDCl_3$) δ 3.20 (1H, m, CH_A H_BN), 3.36 (1H, m, CH_AH_BN), 4.27 (1H, m, O-CH-CH-Ph), 4.32 (2H, q, CH_2CO), 5.35 (1H, d, Ph-CH, J = 5.9 Hz), 5.94 (1H, brs, CONH), 6.64–7.51 (4H, m, Ph-O), 7.37 (5H, m, Ph-C). ESI-MS calcd for $C_{17}H_{17}NO_3Br$ $[M + H]^+$: m/z 362, found 362.

(2S,3S)/(2R,3R)-2-[α-(2-bromophenoxy)benzyl]morpholine (10b) ^{1}H-NMR ($CDCl_3$) δ 2.61 (1H, m, O-CH_AH_BN), 2.78 (3H, m, O-CH_AH_BN-CH_2-), 3.66 (1H, m, O-CH-CH-Ph), 3.95 (2H, m, CH_2CO), 5.20 (1H, d, Ph-CH, J = 5.9 Hz), 6.73–7.47 (4H, m, Ph-O), 7.35 (5H, m, Ph-C). ESI-MS calcd for $C_{17}H_{19}NO_2Br$ $[M + H]^+$: m/z 348, found 348. Anal. calcd for $C_{17}H_{18}NO_2Br{\cdot}0.1H_2O$: C, 58.33; H, 5.24; N, 4.00%; Found: C, 58.63; H, 5.21; N, 4.02%.

Chiral resolution of (R,R)/(S,S)-IPBM and -BPBM by HPLC

Racemic mixtures of IPBM and BPBM containing (S,S) and (R,R) enantiomers were resolved using a Chiralcel OD-H semipreparative column (Chiralcel OD-H, 250×10 mm i.d., Daicel Chemical Industries, Ltd, Osaka, Japan). The column was eluted with hexane:2-propanol:diethylamine=80:20:0.1 at a flow rate of 3.3 ml/min. Then, 20 mg of (R,R)/(S,S)-IPBM was dissolved in a mixture

of hexane:2-propanol=1:1 (2 ml). The retention time of the (R,R) and (S,S) enantiomers of IPBM was 10.8 and 18.5 min, respectively. The (R,R) and (S,S) enantiomers of IPBM were isolated in 86% and 82% yields, respectively. Similarly, the retention time of the (R,R) and (S,S) enantiomers of BPBM were 11.0 and 16.7 min, respectively. The (R,R) and (S,S) enantiomers of BPBM were isolated in 83% and 86% yields, respectively. (S,S)-IPBM: colorless oil; $[a]_D$=−107.5° (*c*=1.40, methanol). (R,R)-IPBM: colorless oil; $[a]_D$=+113.0° (*c*=1.01, methanol). (S,S)-BPBM: colorless oil; $[a]_D$=−79.2° (*c*=1.39, methanol). (R,R)-BPBM: colorless oil; $[a]_D$=+81.2° (*c*=1.59, methanol). Spectroscopic data were the same as those described above for (R,R)/(S,S)-IPBM and -BPBM.

Radiolabelling

The radioiodinated (S,S)-IPBM was obtained by a halogen exchange reaction with sodium $^{125/123}$I-iodine according to the methods of Kiyono et al. [8]. Briefly, (S,S)-BPBM was added to a mixture of sodium $^{125/123}$I-iodine, ammonium sulfate, and copper (II) sulfate pentahydrate in a vial. The reaction mixture was heated for 45 min at 130°C. After cooling, the reaction mixture was extracted with methanol and filtered with a 0.22-μm filter (Ultrafree-MC 0.22-μm filter unit, Millipore Corp., Benford, TX, USA). The filtered extract was applied to a reverse-phase high-performance liquid chromatography (HPLC) column (Cosmosil 5C_{18}-AR-300 Packed Column, 250×10 mm i.d., Nacalai Tesque, Kyoto, Japan), and eluted with 20 m*M* phosphate buffer (pH 2.5):acetonitrile=72:28 at a flow rate of 2.0 ml/min (R_t=42 min for (S,S)-BPBM and 58 min for (S,S)-IPBM). An adequate amount of ethanol was added to the separated (S,S)-$^{125/123}$I-IPBM fraction.

The radiochemical purity of the labeled compound was determined by thin-layer chromatography (TLC) and analytical HPLC. The TLC was performed on a silica gel plate, developed with chloroform: methanol=20:1 (R_f=0.44). Analytical HPLC was performed on a 150×4.6 mm i.d. Cosmosil AR-300 column (Nacalai Tesque, Kyoto, Japan) eluted with 20 m*M* phosphate buffer (pH 2.5):acetonitrile=72:28 at a flow rate of 1.0 ml/min (R_t=15.0 min).

In vitro binding assay

The preparation of the synaptosomal membrane from rat cerebral cortex was carried out according to the methods of Cheetham et al. [18]. Briefly, the cerebral cortex of male Sprague-Dawley rats (10 weeks old) was dissected and homogenized in 30 volumes of ice-cold buffer A (containing 50 m*M* Tris-HCl, 120 m*M* NaCl, and 5 m*M* KCl, pH 7.4) and centrifuged at 28,000 *g* for 10 min at 4°C. The pellet was resuspended in 30 volumes of the same buffer and centrifuged. This procedure was repeated twice with the final pellet being resuspended in 5 volumes of ice-cold buffer B (containing 50 m*M* Tris-HCl, 300 m*M* NaCl, and 5 m*M* KCl, pH 7.4). The suspension was stored at −80°C prior to use. The protein concentration was measured by the Lowry method [19].

^{3}H-nisoxetine competition assays were performed by incubating 400 μl of the cortical membrane (corresponding to 300–400 μg of protein), 50 μl of ^{3}H-nisoxetine (1.0 n*M*), and 50 μl of various concentrations of drugs in buffer B. For ^{3}H-nisoxetine, incubation was performed for 240 min at 4°C. (S,S)-^{125}I-IPBM saturation and competition assays were carried out according to the methods of Choi et al. [20] with slight modifications. In saturation experiments, 400 μl of the cortical membrane (corresponding to 300–400 μg of protein) was mixed with 50 μl of (S,S)-^{125}I-IPBM (0.03–6.4 n*M*). Competition experiments were performed using 50 μl of (S,S)-^{125}I-IPBM (0.06 n*M*) and 50 μl of various concentrations of drugs in buffer B. For (S,S)-^{125}I-IPBM, incubation was carried out for 60 min at 25°C.

At the end of the incubation, the mixture was poured into 4 ml of ice-cold buffer B, rapidly filtered through GF/B fiber filters, and washed with 3×4 ml of buffer B. For ^{3}H-nisoxetine, each filter was placed into a 20-ml scintillation vial containing 8 ml of ACS II (Amersham) and the radioactivity bound to the filter was measured with a liquid scintillation counter (2500-TR, Packard). For (S,S)-^{125}I-IPBM, the radioactivity bound to the filter was measured with a NaI well scintillation counter (Cobra II Auto-Gamma, Packard). Nonspecific binding was determined in the presence of 100 μ*M* nisoxetine. IC_{50} values were determined from displacement curves of the percent inhibition of ^{3}H-nisoxetine or (S,S)-^{125}I-IPBM binding versus the inhibitor concentration using the LIGAND curve-fitting computer program (Elsevier-Biosoft, Cambridge, UK). K_i values were calculated by the method of Cheng and Prusoff [21]. To calculate K_i, the value of 1.0 n*M* reported previously [18] was used as the K_D value of nisoxetine, and the value obtained in this study (1.3 n*M*) was used as the K_D value of (S,S)-IPBM.

Biodistribution in rats

Biodistribution experiments were performed by intravenous administration of (S,S)-^{125}I-IPBM (74 KBq) to 10-week-old male Sprague-Dawley rats. At appropriate time points after the administration, rats were sacrificed by decapitation under light ether anesthesia. Blood and organs were excised and weighed, and the radioactivity was measured with an auto well gamma counter (Aloka ARC2000, Tokyo, Japan).

Ex vivo autoradiographic experiments

Male Sprague-Dawley (10-week-old) rats were intravenously injected with 2.22 MBq of (S,S)-^{125}I-IPBM. At 180 min after the injection, the rats were decapitated under light ether anesthesia, and their brains were rapidly removed, frozen, and cut into sections 20 μm thick with a cryostat microtome. The sections were thaw-mounted on precleaned silane-coated slides. The slides were placed on a Fuji Imaging Plate (BAS-SR, Fuji Photo Film, Japan) for 24 h along with calibrated ^{125}I-labeled external standards (^{125}I-Microscales, Amersham, UK) to obtain (S,S)-^{125}I-IPBM autoradiograms. Densitometric analyses of the autoradiograms were performed using a Bio Imaging Analyzer (BAS3000, Fuji Photo Film, Tokyo, Japan) and Image Gauge (Fuji Photo Film, Tokyo, Japan).

For in vivo blocking experiments, rats were intravenously injected with 2.22 MBq of (S,S)-^{125}I-IPBM and various monoamine transporter-binding agents simultaneously. Nisoxetine (10 mg/kg), fluoxetine (10 mg/kg), and GBR12909 (1 mg/kg) were used as a selective NET-binding agent, a selective SERT-binding agent, and a

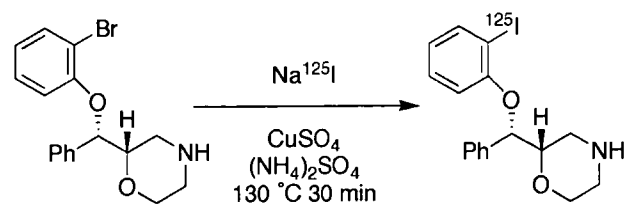

Fig. 3. Radiosynthesis of (S,S)-^{125}I-IPBM

Table 1. Inhibition of ^{3}H-nisoxetine binding to rat brain membranes

Compounds	K_i (nmol/l)
(R,R)/(S,S)-IPBM	10.4±2.64
(S,S)-IPBM	4.22±0.65
(R,R)-IPBM	80.4±18.8
Nisoxetine	1.27±0.03
Desipramine	3.29±0.47
Reboxetine	11.6±1.48

Mean±SD of three independent experiments

selective dopamine transporter (DAT)-binding agent, respectively. The ex vivo autoradiographic procedure was carried out in a similar manner to the control.

SPECT studies

SPECT studies were performed using a HITACHI MEDICO SPECT-2000H-40 gamma camera (Hitachi Medical Co., Tokyo, Japan). A female common marmoset (330 g) was first anesthetized intramuscularly with 20 mg/kg ketamine and 3 mg/kg xylazine. Anesthesia was maintained throughout the study by intraperitoneal injection of sodium pentobarbital. The animal was placed in the SPECT bed and the head was restrained in a stereotaxic apparatus specifically designed for the SPECT scanner. (S,S)-[^{123}I]IPBM (222 MBq) was injected via the saphenous vein, and data acquisition of the brain started as dynamic SPECT scans (360° rotation, 60 s/frame for 32 frames) using low-energy, fan-beam collimators (30% window, 159 keV energy peak, 128×128 matrix mode, pixel size of 1.33 mm) at 0, 35, 70, 105, 140, and 195 min post injection.

Images were reconstructed with a standard filtered back projection algorithm. Regions of interest (ROIs) were placed over different areas of the common marmoset brain with reference to a stereotaxic atlas and magnetic resonance imaging data. Radioactivity, expressed as counts per ml, for each ROI was decay-corrected to the time of injection and corrected for the injection dose.

Statistical analyses

Data are presented as mean values with the SD. Comparisons between groups were performed with the Dunnett multiple comparisons test. A p value <0.05 was considered statistically significant.

Results

Syntheses

(S,S)-IPBM and (S,S)-BPBM were synthesized according to the procedure outlined in Fig. 2. Enantioselective (S,S)-IPBM and (S,S)-BPBM were obtained.

The radiosynthesis of (S,S)-^{125}I-IPBM was achieved with an iodine-bromide exchange reaction (Fig. 3). Following separation from the precursor (S,S)-BPBM using reverse-phase HPLC, (S,S)-^{125}I-IPBM was obtained with no carrier being added. The radiochemical yield was 65%, and the radiochemical purity was greater than 98%.

In vitro binding

Using the reference compounds, nisoxetine, desipramine, and reboxetine, the affinity of racemic IPBM and the (S,S)- and (R,R)-enantiomer of IPBM for brain NET was measured in assays of competition for ^{3}H-nisoxetine-binding sites in rat cortical membranes. The K_i values are summarized in Table 1. Racemic IPBM exhibited approximately the same degree of affinity as its mother compound, racemic reboxetine. The (S,S)-enantiomer showed about two times higher affinity than racemic IPBM, and about 20 times higher than the (R,R)-enantiomer. Moreover, (S,S)-IPBM had a similar affinity to well-known NET-binding agents (nisoxetine and desipramine).

The specific binding of (S,S)-^{125}I-IPBM was saturable with a high affinity and Scatchard transformation of the binding data gave a linear plot indicating one-site binding (Fig. 4). The mean values from four experiments gave a K_D value of 1.30±0.46 n*M*. The selective binding of (S,S)-^{125}I-IPBM to brain NET was measured in competition with various binding agents for norepinephrine, serotonin, and dopamine transporters, using rat cortical membranes. The K_i values are summarized in Table 2. The binding of (S,S)-^{125}I-IPBM was inhibited by nisoxetine and desipramine, selective NET-binding agents. However, (S,S)-^{125}I-IPBM binding was only slightly inhibited by fluoxetine, a selective SERT-binding agent, and hardly inhibited at all by GBR 12909, a selective DAT-binding agent. The selectivity ratio

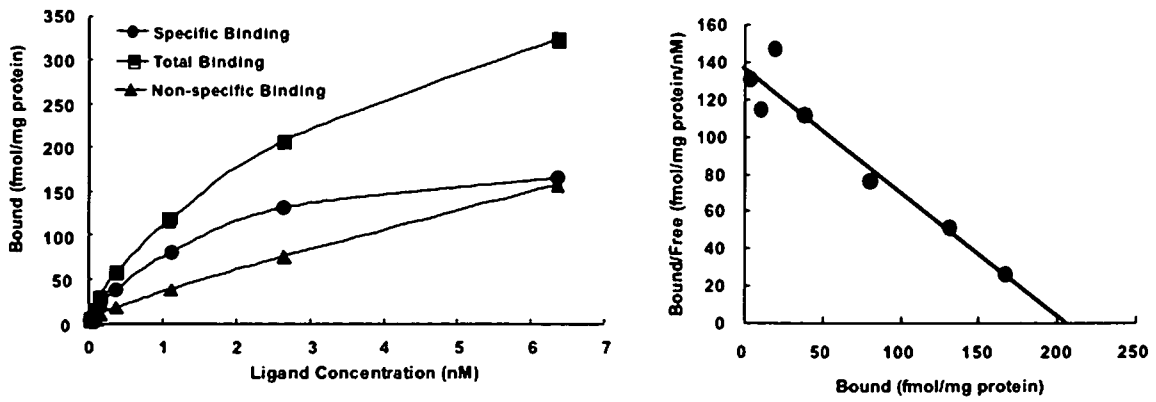

Fig. 4. Scatchard analysis of (S,S)-^{125}I-IPBM binding to rat cortex membrane preparations

Table 2. Inhibition of (S,S)-^{125} I-IPBM binding to rat brain membranes

Compounds	K_i (nmol/l)
Nisoxetine	4.17±1.98
Desipramine	4.99±0.65
Fluoxetine	1,073±437
GBR12909	>5,000

Mean±SD of three independent experiments

of SERT (K_i at SERT/K_i at NET) was 257 and of DAT (K_i at DAT/K_i at NET) was more than 1,000.

Biodistribution in rats

The biodistribution of the radioactivity after intravenous injection of (S,S)-^{125}I-IPBM is shown in Table 3. (S,S)-^{125} I-IPBM rapidly entered the brain, and the level of radioactivity in the brain was highest at 30 min after the injection; it then decreased gradually, although the radioactivity in blood cleared rapidly. The brain-to-blood ratio was 15.9 at 60 min after the injection, and then became stable. A high uptake was observed in the lung, followed by a rapid clearance. The heart and kidneys showed a moderate initial uptake and then a gradual decrease with time. The radioactivity that accumulated in the thyroid and stomach showed no prominent increase until 180 min after the injection.

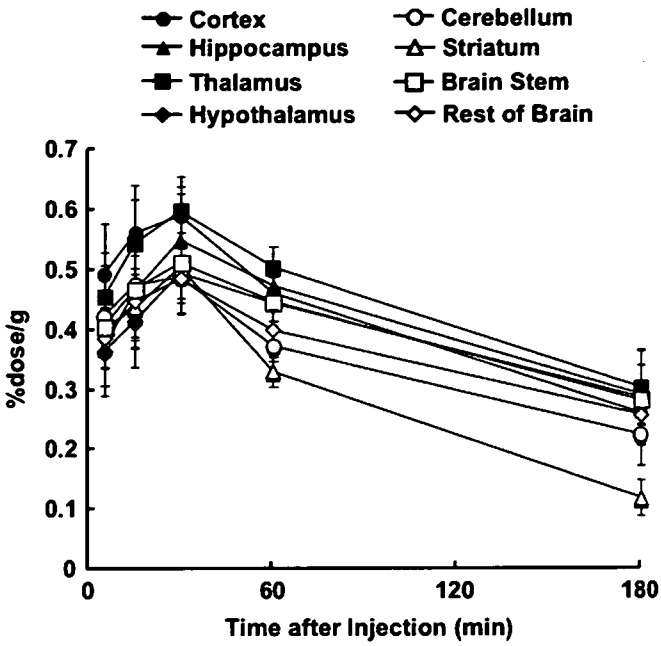

Fig. 5. Regional uptake of (S,S)-^{125}I-IPBM in rat brain. Data are represented as the mean±SD for four rats

Table 3. Biodistribution of (S,S)-^{125} I-IPBM in rats[a]

	Time after injection (min)				
	5	15	30	60	180
Heart	1.06±0.15	0.66±0.13	0.74±0.07	0.64±0.07	0.50±0.13
Lung	5.17±1.26	4.22±1.84	4.41±0.32	2.22±0.80	1.27±0.26
Liver	0.29±0.07	0.20±0.03	0.20±0.02	0.20±0.02	0.15±0.03
Kidney	1.16±0.18	0.91±0.19	0.77±0.08	0.57±0.05	0.30±0.07
Spleen	0.50±0.10	0.96±0.29	1.27±0.20	1.15±0.12	0.74±0.17
Stomach	0.38±0.12	0.51±0.27	0.75±0.07	0.84±0.30	0.63±0.24
Intestine	0.46±0.13	0.92±0.36	1.75±0.06	2.84±0.17	4.49±1.16
Pancreas	0.69±0.07	0.58±0.08	0.58±0.07	0.50±0.07	0.36±0.08
Adrenal	1.37±0.37	1.48±0.23	1.36±0.17	0.78±0.03	0.92±0.59
Thyroid[b]	0.01±0.00	0.01±0.00	0.02±0.00	0.03±0.00	0.04±0.04
Brain	0.44±0.08	0.51±0.08	0.54±0.06	0.43±0.04	0.25±0.05
Blood	0.05±0.01	0.04±0.01	0.04±0.00	0.03±0.00	0.02±0.01
Br/Bld[c]	8.51±0.89	12.4±0.65	14.5±0.65	15.9±0.83	15.4±2.63

[a]Percentage of injected dose/gram tissue (mean±SD for four rats)
[b]Percentage of injected dose/organ (mean±SD for four rats)
[c]Brain-to-blood ratio (percentage of injected ^{125} I dose/gram of organ ratio)

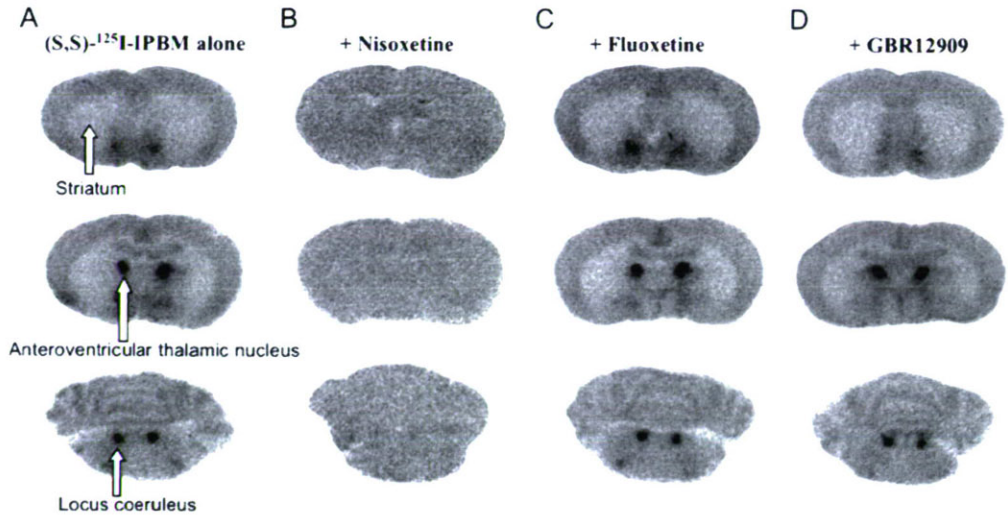

Fig. 6. Ex vivo autoradiograms of rat coronal brain sections at 180 min post injection of (S,S)-^{125}I-IPBM with simultaneous injection of various drugs at a plane passing through the striatum, the anteroventricular thalamic nucleus, and the locus coeruleus. **a** (S,S)-^{125}I-IPBM alone; **b** (S,S)-^{125}I-IPBM plus nisoxetine (10 mg/kg); **c** (S,S)-^{125}I-IPBM plus fluoxetine (10 mg/kg); **d** (S,S)-^{125}I-IPBM plus GBR12909 (1 mg/kg)

The regional distribution of radioactivity in the rat brain is shown in Fig. 5. The accumulation of radioactivity was greater in NET-rich regions, such as the thalamus and cortex, than in the striatum, a NET-poor region [22]. The washout rate was faster in the striatum as compared with other areas. The ratio of radioactivity in other brain regions to that in the striatum was highest at 180 min after injection.

Ex vivo experiments

To investigate in more detail the regional distribution of (S,S)-^{125}I-IPBM in the brain, ex vivo autoradiographic analyses were performed (Fig. 6a). The highest level of radioactivity was observed in the locus coeruleus and anteroventricular thalamic nucleus, which are known to be rich in NET. Conversely, there was less radioactivity in the striatum. The regional distribution of (S,S)-^{125}I-IPBM correlated well with the reported NET expression (r=0.99) (Fig. 7).

Furthermore, effects of various monoamine transporter-binding agents on the cortical uptake of (S,S)-^{125}I-IPBM was studied (Fig. 6b-d). The regional accumulation of radioactivity in the brain at 180 min was determined by conducting ex vivo autographic experiments, and compared with that of the control. The regional accumulation of (S,S)-^{125}I-IPBM is summarized in Fig. 8. The NET-selective agent nisoxetine reduced the accumulation of (S,S)-^{125}I-IPBM to a greater extent in the region where the accumulation of (S,S)-^{125}I-IPBM was higher when administered without drugs, and resulted in almost the same level of accumulation throughout the brain. However, fluoxetine, a SERT-selective agent, and GBR12909, a DAT-selective agent, caused no significant changes in the accumulation.

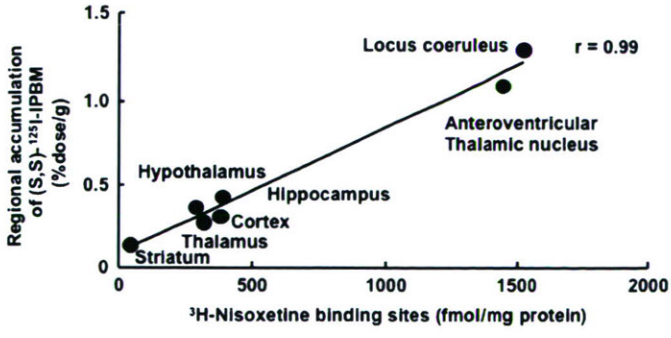

Fig. 7. Correlation between (S,S)-^{125}I-IPBM accumulation determined from ex vivo autoradiograms at 180 min post injection in rats and density of NET sites determined by in vitro ^{3}H-nisoxetine binding [22]

SPECT imaging in the common marmoset

Figure 9 shows SPECT imaging of a common marmoset at 140–172 min and time-radioactivity curves in the cortex, thalamus, cerebellum, and striatum after intravenous injection of (S,S)-^{123}I-IPBM. After injection of (S,S)-^{123}I-IPBM, there was rapid and high level of accumulation of radioactivity in the brain. The elimination rate was different in the various regions, and the accumulation of (S,S)-^{123}I-IPBM in the thalamus was highest. The moderate accumulation was observed in the cortex and cerebellum, but the accumulation of (S,S)-^{123}I-IPBM in the striatum was low. Treatment with nisoxetine (5 mg/kg, i.p.) 68 min after (S,S)-^{123}I-IPBM injection accelerated the elimination rate in the thalamus, cortex, and cerebellum, but not in the striatum. At 211 min after radioligand injection, the radioactivity in the thalamus, cortex, and cerebellum was decreased to that in the striatum.

Discussion

The basic requirements for an effective radiopharmaceutical for the imaging of brain NET include a quantitatively significant uptake in the brain following peripheral administration and a regional cerebral distribution that is correlated with NET density, as well as a high binding affinity and selectivity for the NET protein.

In this study, we succeeded in synthesizing the reboxetine analog (S,S)-IPBM enantioselectively. The affinity of (S,S)-IPBM for brain NET was similar to that of well-known NET-

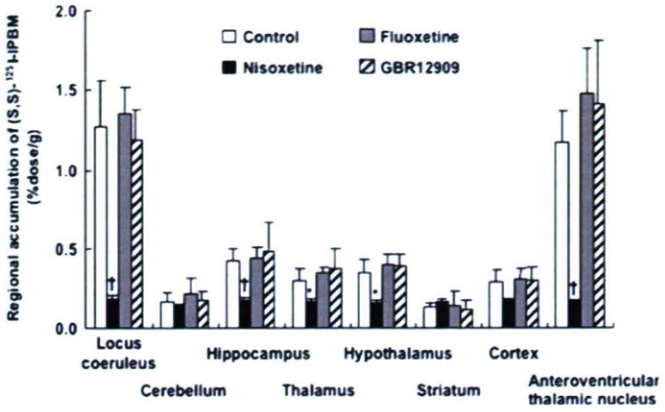

Fig. 8. Effects of various drugs on the regional accumulation of (S,S)-^{125}I-IPBM in rats 180 min post injection measured by ex vivo autoradiography. (S,S)-^{125}I-IPBM was simultaneously injected with each drug. *$p<0.05$ versus control; †$p<0.01$ versus control (Dunnett multiple comparisons test)

binding agents which have high affinity for NET. The affinity of (R,R)/(S,S)-IPBM was similar to that of the mother compound racemic reboxetine, suggesting that the introduction of iodine at position 2 of the phenoxy ring did not affect the affinity for NET, as expected. Moreover, (S,S)-IPBM showed high selectivity for NET. These results suggest that the introduction of iodine at position 2 of the phenoxy ring was suitable.

(S,S)-^{125}I-IPBM showed a rapid and marked accumulation in the brain. The uptake was greater than that of (S,S)-^{11}C-MeNER, a potent PET ligand for brain imaging, and that of (R)-^{125}I-MIPP [(S,S)-^{125}I-IPBM 0.89% ID/organ, (S,S)-^{11}C-MeNER 0.53% ID/organ, and (R)-^{125}I-MIPP 0.45% ID/organ 5 min post injection] [8, 13]. Moreover, the radioactivity in blood was cleared rapidly, and the brain-to-blood ratio, an essential factor for brain imaging, was higher than that of (R)-^{125}I-MIPP [(S,S)-^{125}I-IPBM 15.9 and (R)-^{125}I-MIPP 6.5 at 60 min post injection; (S,S)-^{125}I-IPBM 15.4 and (R)-^{125}I-MIPP 4.7 at 180 min post injection] [8].

In peripheral organs, high uptake was observed in the lungs, heart, and adrenals, in which NET was abundant [23–25]. The level of radioactivity in the thyroid was low, which indicated high stability of (S,S)-^{125}I-IPBM to in vivo deiodination.

Regarding the cerebral distribution of (S,S)-^{125}I-IPBM, a higher midbrain to striatum ratio, which has been used as an index of specific binding [9], was found at 180 min post injection. Furthermore, analyses of (S,S)-^{125}I-IPBM's regional distribution in the brain at 180 min post injection showed a higher accumulation in NET-rich regions, such as the locus coeruleus and anteroventricular thalamic nucleus. The regional distribution of (S,S)-^{125}I-IPBM at 180 min post injection correlated well with the reported NET expression (γ=0.99) (Fig. 9) [22].

In in vivo displacement experiments, the accumulation of (S,S)-IPBM was dramatically decreased to the level in the striatum by the administration of nisoxetine, a NET-selective agent. Furthermore, fluoxetine, a SERT-selective agent, did not affect the accumulation of (S,S)-IPBM. These results indicate that (S,S)-IPBM exhibited more selective binding to NET in vivo than (R)-MIPP.

Imaging studies with SPECT were carried out in the common marmoset. Although the locus coeruleus and anteroventricular thalamic nucleus are too small to be reliably identified with SPECT, (S,S)-^{123}I-IPBM exhibited a regional localization consistent with the known densities of NET in a relatively large area. These images were also similar to those obtained from studies using (S,S)-^{11}C-MeNER, reported recently [26, 27]. The midbrain to striatum ratio reached a plateau 211 min after (S,S)-^{123}I-IPBM injection, and (S,S)-^{123}I-IPBM reached a specific binding equilibrium during the SPECT measurement, indicating that the longer half-life of ^{123}I was suitable for slower kinetics of reboxetine analogs. Furthermore, (S,S)-^{123}I-IPBM accumulation could be displaced by treatment with nisoxetine. These results indicate that the binding of (S,S)-^{123}I-IPBM to brain NET can be visualized with SPECT imaging and that binding of (S,S)-^{123}I-IPBM to NET is reversible.

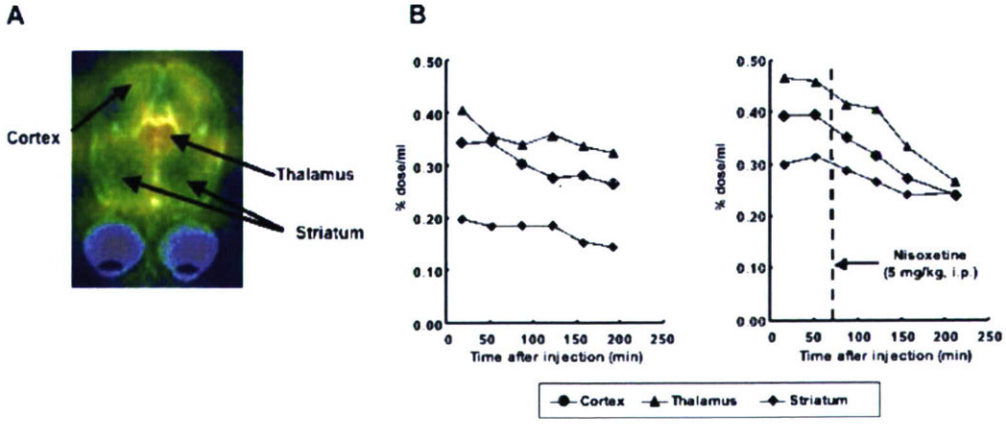

Fig. 9. SPECT images (**a**) and time-radioactivity curves (**b**) of (S,S)-^{123}I-IPBM in the common marmoset brain. Nisoxetine (5 mg/kg) was intraperitoneally administered 68 min after injection

Conclusion

In this study, radioiodinated (S,S)-IPBM, a reboxetine derivative $^{123/125}$I-iodinated at position 2 of the phenoxy ring, was synthesized. In vitro competitive binding experiments showed a high affinity and selectivity of (S,S)-IPBM for brain NET. In vivo biodistribution experiments demonstrated that (S,S)-^{125}I-IPBM showed good uptake in the brain, and a regional cerebral distribution in association with NET. Furthermore, (S,S)-^{123}I-IPBM allowed visualization of brain NET in the common marmoset with SPECT. Thus, (S,S)-^{123}I-IPBM is a potential radioligand for imaging brain NET.

Acknowledgements. We would like to thank Daiichi Radioisotope Laboratories Ltd., Tokyo, Japan, for providing Na^{123}I. This study was supported in part by Grants-in-aid for General Scientific Research from the Ministry of Education, Culture, Sports, Science and Technology of Japan and the 21st Century COE Program "Knowledge Information Infrastructure for Genome Science".

References

1. Blakely RD, De Felice LJ, Hartzell HC. Molecular physiology of orepinephrine and serotonin transporters. J Exp Biol 1994;196:263–281
2. Schomig E, Fischer P, Schonfeld CL, Trendelenburg U. The extent of neuronal re-uptake of ^{3}H-noradrenaline in isolated vasa deferentia and atria of the rat. Naunyn Schmiedebergs Arch Pharmacol 1989;340:502–508
3. Ryu SH, Lee SH, Lee HJ, Cha JH, Ham BJ, Han CS, et al. Association between norepinephrine transporter gene polymorphism and major depression. Neuropsychobiology 2004;49:174–177
4. Klimek V, Stockmeier C, Overholser J, Meltzer HY, Kalka S, Dilley G, et al. Reduced levels of norepinephrine transporters in the locus coeruleus in major depression. J Neurosci 1997;17: 8451–8458
5. Brunello N, Mendlewicz J, Kasper S, Leonard B, Montgomery S, Nelson J, et al. The role of noradrenaline and selective noradrenaline reuptake inhibition in depression. Eur Neuropsychopharmacol 2002;12:461–475
6. Marien MR, Colpaert FC, Rosenquist AC. Noradrenergic mechanisms in neurodegenerative diseases: a theory. Brain Res Brain Res Rev 2004;45:38–78
7. Tejani-Butt SM, Yang J, Zaffar H. Norepinephrine transporter sites are decreased in the locus coeruleus in Alzheimer's disease. Brain Res 1993;631:147–150
8. Kiyono Y, Kanegawa N, Kawashima H, Kitamura Y, Iida Y, Saji H. Evaluation of radioiodinated (R)-N-methyl-3-(2-iodophenoxy)-3-phenylpropanamine as a ligand for brain norepinephrine transporter imaging. Nucl Med Biol 2004;31:147–153
9. Kung MP, Choi SR, Hou C, Zhuang ZP, Foulon C, Kung HF. Selective binding of 2-[^{125}I]iodo-nisoxetine to norepinephrine transporters in the brain. Nucl Med Biol 2004;31:533–541
10. Chumpradit S, Kung MP, Panyachotipun C, Prapansiri V, Foulon C, Brooks BP, et al. Iodinated tomoxetine derivatives as selective ligands for serotonin and norepinephrine uptake sites. J Med Chem 1992;35:4492–4497
11. Gehlert DR, Schober DA, Hemrick-Luecke SK, Krushinski J, Howbert JJ, Robertson DW, et al. Novel halogenated analogs of tomoxetine that are potent and selective inhibitors of norepinephrine uptake in brain. Neurochem Int 1995;26:47–52
12. Millan MJ, Gobert A, Lejeune F, Newman-Tancredi A, Rivet JM, Auclair A, et al. S33005, a novel ligand at both serotonin and norepinephrine transporters: I. Receptor binding, electrophysiological, and neurochemical profile in comparison with venlafaxine, reboxetine, citalopram, and clomipramine. J Pharmacol Exp Ther 2001;298:565–580
13. Wilson AA, Johnson DP, Mozley D, Hussey D, Ginovart N, Nobrega J, et al. Synthesis and in vivo evaluation of novel radiotracers for the in vivo imaging of the norepinephrine transporter. Nucl Med Biol 2003;30:85–92
14. Ding YS, Lin KS, Garza V, Carter P, Alexoff D, Logan J, et al. Evaluation of a new norepinephrine transporter PET ligand in baboons, both in brain and peripheral organs. Synapse 2003;50: 345–352
15. Schou M, Halldin C, Sovago J, Pike VW, Gulyas B, Mozley PD, et al. Specific in vivo binding to the norepinephrine transporter demonstrated with the PET radioligand, (S,S)-[^{11}C] MeNER. Nucl Med Biol 2003;30:707–714
16. Schou M, Halldin C, Sovago J, Pike VW, Hall H, Gulyas B, et al. PET evaluation of novel radiofluorinated reboxetine analogs as norepinephrine transporter probes in the monkey brain. Synapse 2004;53:57–67
17. Melloni P, Della Torre A, Lazzari E, Mazzini G, Meroni M. Configurational studies on 2-[α-(2-ethoxyphenoxy)benzyl] morpholine FCE 20124. Tetrahedron 1985;41:1393–1399
18. Cheetham SC, Viggers JA, Butler SA, Prow MR, Heal DJ. [^{3}H] nisoxetine—a radioligand for noradrenaline reuptake sites: correlation with inhibition of [^{3}H]noradrenaline uptake and effect of DSP-4 lesioning and antidepressant treatments. Neuropharmacology 1996;35:63–70
19. Lowry OH, Rosebrough NJ, Farr AL, Randall RJ. Protein measurement with the Folin phenol reagent. J Biol Chem 1951; 193:265–275
20. Choi SR, Hou C, Oya S, Mu M, Kung MP, Siciliano M, et al. Selective in vitro and in vivo binding of [^{125}I]ADAM to serotonin transporters in rat brain. Synapse 2000;38:403–412
21. Cheng Y, Prusoff WH. Relationship between the inhibition constant (K_i) and the concentration of inhibitor which causes 50 per cent inhibition (IC_{50}) of an enzymatic reaction. Biochem Pharmacol 1973;22:3099–3108
22. Tejani-Butt SM. [^{3}H]nisoxetine: a radioligand for quantitation of norepinephrine uptake sites by autoradiography or by homogenate binding. J Pharmacol Exp Ther 1992;260:427–436
23. Tseng YT, Padbury JF. Expression of a pulmonary endothelial norepinephrine transporter. J Neural Transm 1998;105:1187–1191
24. Kiyono Y, Kanegawa N, Kawashima H, Fujiwara H, Iida Y, Nishimura H, et al. A new norepinephrine transporter imaging agent for cardiac sympathetic nervous function imaging: radioiodinated (R)-N-methyl-3-(2-iodophenoxy)-3-phenylpropanamine. Nucl Med Biol 2003;30:697–706
25. Toyohira Y, Yanagihara N, Minami K, Ueno S, Uezono Y, Tachikawa E, et al. Down-regulation of the noradrenaline transporter by interferon-alpha in cultured bovine adrenal medullary cells. J Neurochem 1998;70:1441–1447
26. Ding YS, Lin KS, Logan J, Benveniste H, Carter P. Comparative evaluation of positron emission tomography radiotracers for imaging the norepinephrine transporter: (S,S) and (R,R) enantiomers of reboxetine analogs ([^{11}C]methylreboxetine, 3-Cl-[^{11}C]methyl-reboxetine and [^{18}F]fluororeboxetine), (R)-[^{11}C]nisoxetine, [^{11}C]oxaprotiline and [^{11}C]lortalamine. J Neurochem 2005;94:337–351
27. Logan J, Ding YS, Lin KS, Pareto D, Fowler J, Biegon A. Modeling and analysis of PET studies with norepinephrine transporter ligands: the search for a reference region. Nucl Med Biol 2005;32:531–542

Invited Review Article

Chemical Control of Biological Activity and Biodistribution of Metal Compounds : Drug Design of Metal Complexes with Biological Activity and Target-Specific Biodistribution

Hideo Saji[1], Kazuma Ogawa[2], Youji Kitamura[3], Megumi Kubota-Akizawa[1] and Hidekazu Kawashima[1]

[1] Department of Patho-functional Bioanalysis, Graduate School of Pharmaceutical Sciences, Kyoto University, Kyoto 606-8501, Japan
[2] Central Institute of Radioisotopes Science, Division of Tracer Kinetics, Advanced Science Research Center, Kanazawa University, Kanazawa 920-8640, Japan
[3] Graduate School of Medicine and Dentistry and Pharmaceutical Sciences, Okayama University, Okayama 700-8558, Japan

Abstract

The development of metallic compounds for the diagnosis and therapy of diseases has been expected to open a new field of medicinal science. These compounds are required to exhibit biological activity and a specific localization to the target tissue. These demands constitute a great challenge on the rational design of metallic compounds and we have proposed two approaches, a pendant approach and an integrated approach in order to achieve this purpose. The pendant approach involves designing a biologically active compound by the attachment of a chelating group for binding the metal ion to a mother compound without the effect on the inherent biospecificity of the mother compound. A typical example of the pendant approach is bifunctional radiopharmaceuticals used for nuclear medical diagnosis and internal radiotherapy. The integrated approach involves designing a metallic compound with a biologically activity and physicochemical properties suitable for target-specific delivery by coordination to a mother compound with metal ion.

This review will describe our recent progress in research on a bifunctional radiopharamceutical labeled with metallic radionuclides, Rhenium-186 for therapy of painful bone metastases as an example of the pendant approach and a lipophilic zinc complex with protective effect against ischemic neuronal injury as an example of the integrated approach.

Keywords : metallic compound, drug design, bifunctional radiopharmaceutical, rhenium-186, bisphosphonates, zinc, neuroprotection.

1. Introduction

Many metallic compounds have biological activities, but the application of these compounds in the medical field has been limited. The development of metallic compounds for the diagnosis and treatment of diseases has been expected to open a new field of medicinal science. However, metallic compounds are required to exhibit biologically appropriate activity and a specific localization to target tissue. To obtain such compounds, we have proposed two approaches, a pendant approach and an integrated approach (Fig. 1).

The pendant approach involves designing a compound containing independent groups both with the ability to deliver into the targeted tissue/organ and with the ability to bind metallic ions. In the pendant approach, compounds with a radiometallic nuclide for nuclear medical diagnosis and internal radiotherapy, called "bifunctional

Address correspondence to :
Hideo Saji, Ph.D.
Department of Patho-Functional Bioanalysis, Graduate School of Pharmaceutical Sciences, Kyoto University, Yoshida Shimoadachi-cho, Sakyo-ku, Kyoto 606-8501, Japan
TEL : +81-75-753-4556
FAX : +81-75-753-4568
E-mail : hsaji@pharm.kyoto-u.ac.jp

Received : 20 October 2006
Accepted : 2 March 2007

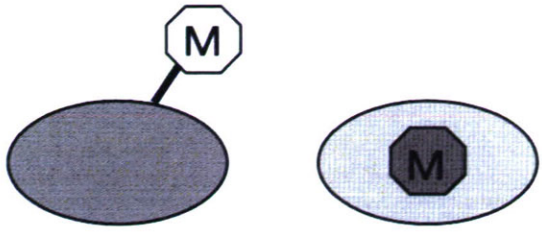

Fig. 1 Concept of the pendant approach and integrated approach.

radiopharmaceuticals", are of particular interest [1-3].

The integrated approach involves designing metallic compounds with physicochemical properties suitable for targeted delivery. A typical example is the development of a lipophilic metallic compound for improving the ability to penetrate the blood-brain barrier [4-6]. Another example is raising the water-solubility to prompt renal excretion.

This review will describe recent progress in our research into bifunctional radiopharmaceuticals labeled with metallic radionuclides for therapy as an example of the pendant approach and a lipophilic zinc complex with a protective effect against ischemic neuronal injury as an example of the integrated approach.

2. Pendant approach

2.1 Concept of the pendant approach : Bifunctional radiopharmaceutical

Nuclear medicine is a diagnostic tool used to visualize changes in physiological and biochemical processes throughout living tissues and organs as well as in regional anatomy (Fig. 2). Furthermore, nuclear medicine has applications to therapy, based on the radiation of radioactive nuclides. Drugs containing radioactive nuclides to be used in nuclear medicine are called radiopharmaceuticals. Radiopharmaceuticals are required to have certain biological properties : a high level of radioactivity localized to the target tissue and a high target/non-target tissue ratio for clear imaging or effective therapy.

The radioactive nuclides used in diagnostic nuclear medicine are short-lived, low gamma energy emitters. In internal radiotherapy, beta- or alpha particle emitters, which provide high radiation doses, are useful as therapeutic radionuclides. The radionuclides used for these purposes include some radioisotopes of metallic elements. Thus, the great demand for biospecific metallic radiopharamceuticals has evolved into the rational design of so called "bifunctional radiopharmaceuticals" ; that is, a radiopharmaceutical containing a group for the selective targeting of diseased tissue together with a group with the ability to bind radiometallic nuclides [1-3] (Fig. 3). Research on bifunctional radiopharmaceuticals started with the development of radiolabeled macromolecules, such as proteins [1,7,8]. In recent years, bifunctional radiopharmaceuticals have also been used for the labeling of non-protein compounds such as peptides and drugs of low molecular weight [1,9,10].

The pendant approach involves hanging the metal complexing moiety from the main body of the molecule responsible for delivery to the target site. The key to this design for small molecules is the strategic placement of the radiometal-chelate-tether moiety at a site on the ligand toward which the molecule responsible for biological function is sterically tolerant.

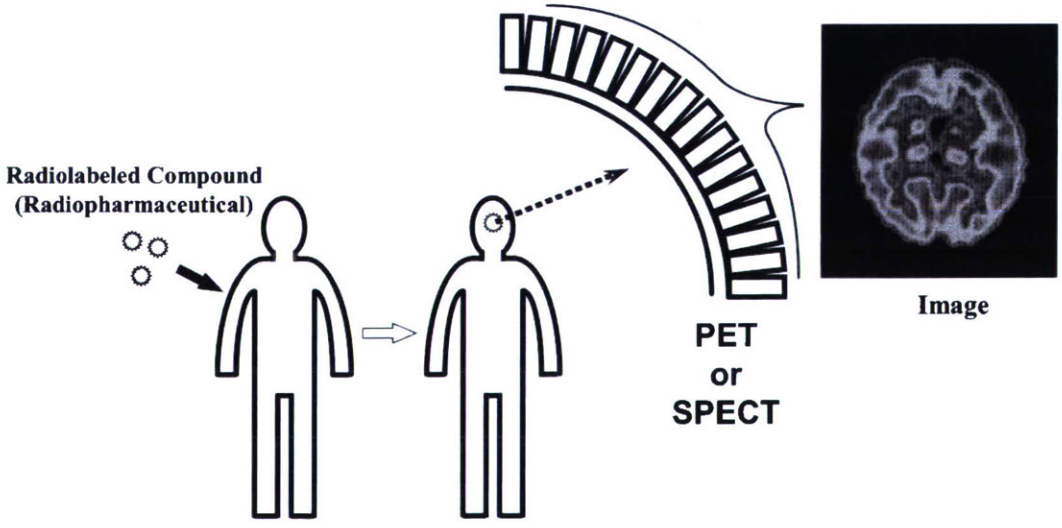

Fig. 2 Targeted imaging system (diagnostic nuclear medicine)

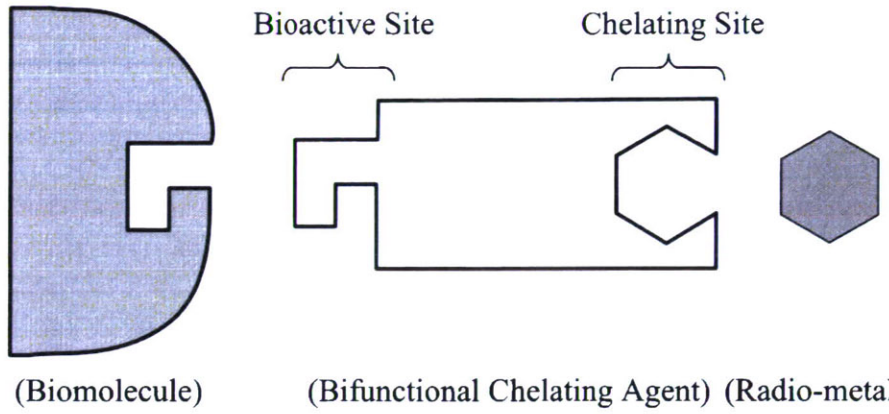

Fig. 3 Bifunctional radiopharmaceutical.
A molecule holding two reactive sites for binding the biomolecule and chelating the radiometal is called a bifunctional chelating agent.

2.2 Development of Rhenium-186-chelate-conjugated Bisphosphonates for painful bone metastases

Malignant tumors frequently metastasize to the bone. A prominent symptom of these metastases is pain, which affects the patient's quality of life, and is an important clinical problem [11]. Localized radiation therapy is an effective modality for localized lesions, providing palliation of bone pain, however, a common problem in patients with bone metastases is the development of multiple sites of metastasis, and so internal radiotherapy using specifically localized beta emitters is preferable [12]. Recently, $^{89}SrCl_2$ has been used as a palliative agent for painful osseous metastases. However, ^{89}Sr is a pure beta emitter and has a relatively long half-life (50.5 d). These physical properties could be a disadvantage for clinical use. The use of Rhemium-186-1-hydroxyethylidene-1,1-diphosphonate (^{186}Re-HEDP) has also been proposed for the palliation of metastatic bone pain [13]. ^{186}Re is a promising radionuclide with a maximum beta emission of 1.07 MeV and gamma ray emission of 137 keV (9%), making it adequate for therapy and imaging, respectively. Furthermore, the physical half-life of ^{186}Re is 3.8 days, which is adequate for shipment and processing of the radiopharmaceutical but not too long for the disposal of radioactive waste. However, it has reported that ^{186}Re-HEDP shows a delayed blood clearance and high gastric uptake due to the poor stability of the ^{186}Re complex in vivo leading to the generation of ^{186}Re-perrhenate ($^{186}ReO_4^-$) [14,15]. Furthermore, though the accumulation in bone as a definitive factor of therapeutic effect is more important, the instability of ^{186}Re-HEDP described above may decrease the bone uptake.

Thus, based on the idea of bifunctional radiopharmaceuticals, we developed a novel ^{186}Re-chelate-conjugated bisphosphonate (^{186}Re-MAMA-BP, Fig. 4-A), introducing a highly stable ^{186}Re-MAMA complex to improve the instability of ^{186}Re-HEDP [16].

To evaluate the stability of ^{186}Re complexes in vitro, ^{186}Re-MAMA-BP and ^{186}Re-HEDP were incubated in phosphate-buffered saline. After 24 hours of incubation, about 80% of the ^{186}Re-MAMA-BP remained intact, compared to only about 30% of the ^{186}Re-HEDP. This is because the ^{186}Re-HEDP was degraded to $^{186}ReO_4^-$ with time. In biodistribution experiments in mice, ^{186}Re-MAMA-BP showed a significantly lower uptake by the stomach than ^{186}Re-HEDP. Since ReO_4^- is known to accumulate in the stomach, accumulation in the stomach is an index of the decomposition of a Re-complex in biodistribution studies. Then, a lower level of ^{186}Re-MAMA-

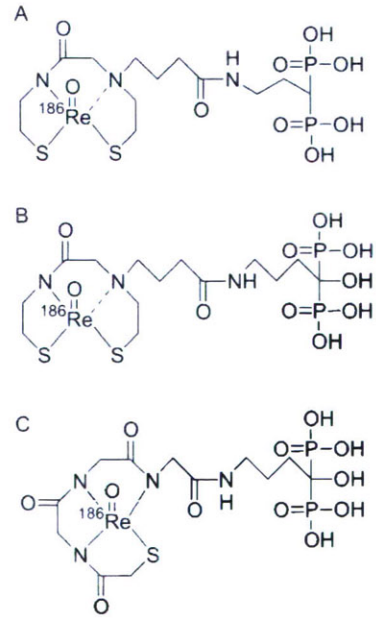

Fig. 4 Structures of ^{186}Re-MAMA-BP (A), ^{186}Re-MAMA-HBP (B), and ^{186}Re-MAG3-HBP (C).

BP in the stomach indicates better stability in vivo.

Meanwhile, ^{186}Re-MAMA-BP showed a faster clearance from the blood than did ^{186}Re-HEDP (Fig. 5-A). It was reported that the ^{186}Re-HEDP complex gave rise to $^{186}ReO_4^-$ in vivo and the clearance from blood of $^{186}ReO_4^-$ was slower than that of ^{186}Re-HEDP. It is suggested that the more rapid clearance from the blood of ^{186}Re-MAMA -BP is responsible for its stability, when compared with ^{186}Re-HEDP. Furthermore, ^{186}Re-MAMA-BP showed a rapid accumulation and long residence in the bone, and its uptake by the bone was significantly greater than that of ^{186}Re-HEDP (Fig. 5-B). The better accumulation of ^{186} Re-MAMA-BP in bone would be partly caused by its greater stability.

Bisphosphonates have been widely used as inhibitors of bone resorption for the treatment of bone diseases and extensively investigated [17]. All bisphosphonates contain two phosphonate groups attached to a single carbon atom, forming a P-C-P structure, and this central carbon has various side chains. It was reported that bisphosphonates containing a hydroxy group have higher affinity for bone mineral [18]. We supposed that the therapeutic effect of ^{186}Re complex-conjugated bisphosphonate could be increased by the introduction of a hydroxy group, then we developed ^{186}Re-MAMA-HBP (Fig. 5-B) [19]. To investigate the affinity for bone in vitro, a hydroxyapatite-binding assay was performed. As expected, ^{186}Re-MAMA-HBP showed a greater affinity for hydroxyapatite beads than did ^{186}Re-MAMA-BP (Fig. 6). This result was reflected by its behavior in vivo. In biodistribution experiments, more ^{186}Re-MAMA-HBP than ^{186}Re-MAMA-BP accumulated in bone. These findings suggest that a hydroxyl group at the central carbon in the design of ^{186}Re-chelate-conjugated bisphosphonates plays a critical role in the enhancement of bone accumulation.

^{186}Re-MAMA-HBP showed the desired properties, namely, greater accumulation in the bone and rapid clearance from the blood. However, hepatic radioactivity levels were significantly higher after the administration of ^{186}Re-MAMA-HBP and ^{186}Re-MAMA-BP than ^{186}Re-HEDP (Fig. 5-C), possibly caused by the increase in lipophilicity with the introduction of the ^{186}Re-MAMA complex into the bisphosphonate structure.

Thus, we developed a ^{186}Re-labeled MAG3-conjugated bisphosphonate (^{186}Re-MAG3-HBP, Fig. 4-C) to modify the physicochemical characteristics of ^{186}Re-MAMA-HBP and ^{186}Re-MAMA-BP and to reduce their hepatic uptake [20]. MAG3 was selected as the ^{186}Re-chelating group because it could form a stable and more hydrophilic complex with ^{186}Re.

^{186}Re-MAG3-HBP also showed good stability in buffered solution. After 24 hours of incubation, about 95% of ^{186}Re-MAG3-HBP remained intact. In biodistribution experiments, ^{186}Re-MAG3-HBP also showed a much higher accumulation in the bone and a faster clearance from the blood than did ^{186}Re-HEDP (Fig. 5-A,B). Furthermore, hepatic radioactivity levels were significantly lower after the administration of ^{186}Re-MAG3-HBP than of ^{186}Re-MAMA-HBP and ^{186}Re-MAMA-BP (Fig. 5-C). The results of the biodistribution experiments and partition coefficients (^{186}Re-MAMA-BP : -0.96±0.01, ^{186}Re-MAMA -HBP : -1.02±0.01, and ^{186}Re-MAG3-HBP : -2.68±0.01, respectively) indicated that the high hepatic uptake of ^{186} Re-MAMA-conjugated bisphosphonates was attributable to the physicochemical properties of the ^{186}Re-MAMA complex.

In summary, we developed highly stable ^{186}Re-chelate-conjugated bisphosphonates, ^{186}Re-MAMA-BP, ^{186}Re-MAMA-HBP, and ^{186}Re-MAG3-HBP. These agents showed higher bone : blood ratios of radioactivity in mice than did ^{186}Re-HEDP, resulting from greater accumulation in the bone and rapid clearance from the blood.

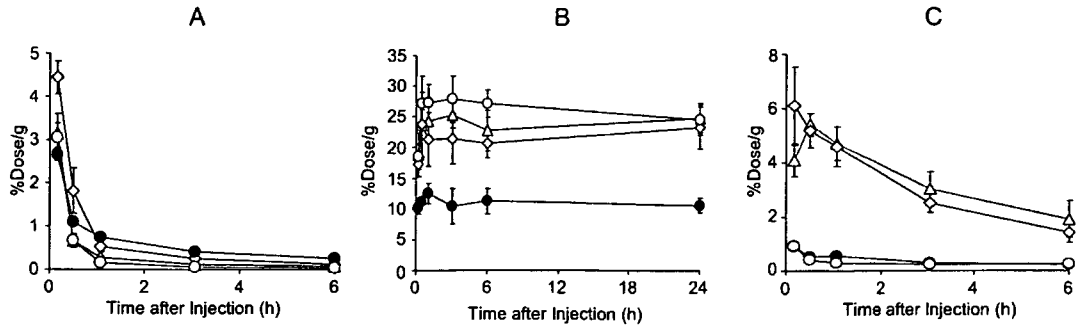

Fig. 5 Biodistribution (A : Blood, B : Bone, C : Liver) of ^{186}Re-MAMA-BP (open diamonds), ^{186}Re-MAMA-HBP (open triangles), ^{186}Re-MAG3-HBP (open circles), and ^{186}Re-HEDP (closed circles) in mice.

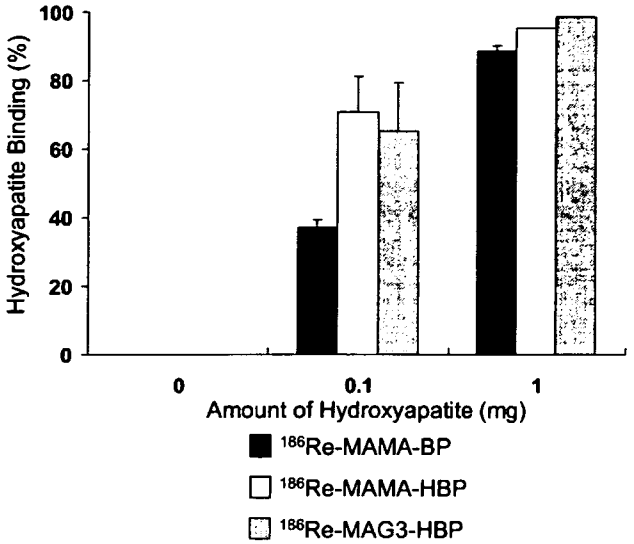

Fig. 6 Binding to hydroxyapatite of ^{186}Re-MAMA-BP, ^{186}Re-MAMA-HBP, and ^{186}Re-MAG3-HBP.

Among these ^{186}Re-chelate-conjugated bisphosphonates, ^{186}Re-MAG3-HBP showed a superior biodistribution as a bone-seeking agent because of its high selectivity for bone as a target tissue. The present findings would provide useful information on the drug design of bone-seeking therapeutic radiopharmaceuticals.

3. Integrated approach

3.1 Concept of integrated approach

The integrated approach involves the incorporation of a group containing physicochemical properties suitable for targeted delivery into a biologically active metal complex, resulting in both an improvement in biodistribution and the preservation of the biological activity of the metallic compound[1]. However, this design often results in a more synthetically challenging target molecule, and the challenge of maintaining biological activity is often greater as well.

2.2 Development of a highly membrane permeable zinc complex providing protection against ischemic neuronal injury.

2.2.1 Studies on the movement and effect of vesicular zinc in brain ischemia

The brain contains an abundant amount of zinc, particularly in the hippocampus, cerebral cortex, and limbic system[21]. About 10% of all zinc in the brain exists in the presynaptic vesicles of glutamatergic neurons and is released into synaptic clefts upon the excitation of nerves [22,23]. On the other hand, the influx of calcium through *N*-methyl-D-asparate (NMDA) receptors induced by glutamate, which is excessively released from glutamatergic nerve terminals into synaptic clefts during brain ischemia, is thought to relate with neuronal death after ischemia. In addition, some studies reported that zinc inhibits NMDA receptors by interacting with the zinc-binding site on the receptors [24]. These studies suggest that zinc, which is released from synaptic vesicles during brain ischemia along with glutamate, may exert a protective effect against glutamate-induced neuronal injury by blocking the influx of calcium via NMDA receptors. Conversely, many reports have indicated that an excessive amount of synaptic vesicular zinc is released during forebrain ischemia, and the released zinc might cause delayed neuronal death after ischemia [25]. Thus, there are conflicting reports about the effect of synaptic vesicular zinc on ischemic neuronal injury, and so the exact role of vesicular zinc is still unclear. One of the key points of this argument is the concentration of zinc released during ischemia, but there have been few reports that describe the effect of zinc based on its concentration directly determined *in vivo*. Therefore, we investigated the movement and effect of zinc in ischemia based on quantity *in vivo*.

First, the effect of various concentrations of zinc on glutamate-induced calcium influx and neuronal death were examined in cultured hippocampal neurons [26]. The addition of a low concentration (under 100 μM) of zinc inhibited both glutamate-induced calcium influx and neuronal death. In contrast, a higher concentration (over 150 μM) of zinc decreased neuronal viability although calcium influx was still inhibited, which means that a high concentration of zinc exerts its own neurotoxicity. These results indicate that zinc exhibits biphasic effects depending on its concentration. On the other hand, co-addition of glutamate and Ca-EDTA, which binds extracellular zinc, increased glutamate-induced calcium influx and aggravated the neurotoxicity of glutamate. These results suggest that, in cultured neurons, vesicular zinc was released by glutamate and the concentration released might be low, exhibiting a neuroprotective effect against the neurotoxicity of glutamate.

To investigate the movement and effect of vesicular zinc in a model of ischemia, we investigated the temporal change to extracellular zinc and glutamate levels in the cortex using microdialysis in rats with middle cerebral artery occlusion (MCAO) [27,28]. The microdialysis experiment revealed that the extracellular concentration of zinc in the cortex increased transiently reaching a peak 30 min after occlusion, then decreased with time, returning to the basal level after reperfusion (Fig. 7). This time